Nonlinear deformation behaviour of auxetic cellular materials with re-entrant lattice structure

Nonlinear deformation behaviour of auxetic cellular materials with re-entrant lattice structure

Journal:	*Fatigue & Fracture of Engineering Materials & Structures*
Manuscript ID	FFEMS-6140.R1
Manuscript Type:	Revised Contribution
Date Submitted by the Author:	n/a
Complete List of Authors:	Brighenti, Roberto; University of Parma, Dept. of Civil Engng Environment & Architecture Spagnoli, Andrea; University of Parma, Dept Civil Engng LANFRANCHI, Matteo; University of Parma, Dept Civil Engng Soncini, Francesco; University of Parma, Dept Civil Engng
Keywords:	Metamaterials, Auxetic behaviour, Smart structures, Re-entrant lattice structure

Nonlinear deformation behaviour of auxetic cellular materials with re-entrant lattice structure

Roberto BRIGHENTI, Andrea SPAGNOLI, Matteo LANFRANCHI, Francesco SONCINI

Department of Civil and Environmental Engineering & Architecture
University of Parma, Parco Area delle Scienze 181/A, 43124 Parma, Italy

* *Corresponding author: E-mail: brigh@unipr.it, Phone +39 0521 905910, Fax +39 0521 905924*

Abstract

Recent frontiers in material development are represented by a class of so-called auxetic metamaterials that, thanks to their structure rather than composition, are characterised by a negative Poisson's ratio. In the present paper a two dimensional auxetic plate, made by structural straight elements forming a lattice periodic structure with re-entrant cells, is considered. A thorough discussion on the linear and geometrically non-linear deformability of the auxetic plate is presented. The key geometric parameters governing the deformability of the plate are identified and some analytical expressions for calculating the Poisson's ratio, as a function of the applied strain, are given. Numerical (finite element) analyses and experimental tests on 3-D printed specimens are carried out to verify the theoretical findings. For the latter ones, full field strain maps are obtained by means of a suitable interpolation of the sampled displacement field measured by digital image techniques.

Keywords: Metamaterials, Auxetic behaviour, Smart structures, Re-entrant lattice structure.

1. Introduction

So-called metamaterials, obtained through the proper design of their microstructure, can exhibit particular mechanical properties corresponding to a smart behaviour. Among the large class of metamaterials, auxetic materials – i.e. materials with a negative Poisson's ratio (NPR) – are characterized by an uncommon mechanical behaviour since they show an opposite tendency, with respect to traditional ones: they transversally expand when stretched and contract when compressed[1]. Their behaviour is opposite to those exhibited by the incompressible materials, such as rubbers for which the Poisson's ratio tends to 0.5, and for this reason are also called anti-rubber materials. Such an uncommon behaviour is usually determined by the material's structure (at the micro or mesoscale) rather than by its composition.

Typically the applications where NPR materials are involved, are mainly based on the exploitation of their high toughness, resilience, shear resistance that assume relevant values with respect to others traditional class of solids. In fact auxetic materials are usually characterized by good shear resistance[2-4], indentation resistance[5], noticeable fracture toughness[6], relevant sound and vibration absorption[7,8], high load-carrying capacity due to friction in joints operating under shear loads[9]. It can easily be argued that the negative value of the Poisson's ratio has relevant effects in term of kinematics and deformation of structural elements, and heavily influences the distribution of strains and stresses. As a matter of fact, NPR materials can reduce the stress concentration factor at geometrical discontinuities, enhance the performance of piezoelectric transducers, improve the behaviour of fasteners, bumpers, sound proofing systems and so on[10].

Other relevant applications of NPR materials, are in the biomedical field where the exploitation of the auxetic property is made in the production of hollow pipes for artery opening, obtained by the lateral expansion under tension of such elements and in the mechanical characteristics of surgical implants[11,12]. Suture or muscle/ligament anchors can benefit from these materials as well as for the productions of scaffolds with porous structures, typical of auxetic materials, for tissue regeneration purpose[13,14].

A relevant property of NPR materials can be observed under bending actions: in fact it is well known as traditional materials deform by assuming a configuration that correspond to shrink in the direction perpendicular to the bending plane (anticlastic curvature), while auxetic ones are characterized by an opposite curvature of the edges, i.e. a convex shape occurs (dome-like pattern, occurring in the same direction of the bending force, synclastic curvature). This particular deformation shape can be considered in the design of smart textiles allowing to follow the synclastic double curvatures of the human body, and enables to produce elements which easily conform to shapes normally required in the automotive and aerospace industries[15-16].

More traditional engineering applications can also have relevant advantages from the use of NPR materials: fibre reinforced composites with auxetic reinforcement (auxetic fibres easily resist to pull-out thanks to the expansion when stretched), smart fasteners and rivets, structural elements with high impact and indentation strength, high shock and sound energy absorption[17-21], fasteners and tuneable filters, materials for high technology packing, knee and elbow pads, etc.

A relevant aspect concerning the NPR materials is that, typically, their auxeticity does not depend on the size scale of the structural component, leading to the possibility to design auxetic "expandable" elements, usefully adopted to realize space structures such as antennas and shields: they have a compact shape and self-contained volume until they "open up" when tensioned in their final destination place[22].

It is worth mention that the design and production of materials having these unusual properties is nowadays possible; materials with NPR property, such as microporous polymers, metallic foams, auxetic fibres and rivets, paper sheets, natural materials (such as bone, e.g. see Ref. 23), in the last decades have been recognized, designed or produced[24].

In the present paper a brief introduction on auxetic materials is presented by underlying their potentiality in the design of structural elements. Then, a metamaterial plate, obtained by assembling elementary auxetic cells with different geometrical parameters, is considered: both numerical analyses and experimental tests are performed on such an auxetic sheet and the results are compared. A thourough discussion about the obtained structural response in terms of linear and geometrically nonlinear deformability is given. Some preliminary results have been presented in Ref. 25.

2. An auxetic material with re-entrant lattice structure

In the present study a lattice-like 2-D auxetic sheet is considered; its unit cell is characterised by a re-entrant double arrow shape as shown in Fig. 1.

Fig. 1. Geometrical characteristics of the elementary auxetic cell (a). Structural scheme of the cell (b).

2.1 Mechanical modeling of the elementary cell

The geometrical properties of the elementary cell are defined by three parameters, e.g. the reference length a_0 and the two angles α_0, β_0. On the basis of these three geometrical parameters, all the relevant dimensions of the cell can be deduced:

$$l_{0x} = a_0 cos\alpha_0, \qquad l_{0y} = 2a_0 sen\alpha_0, \qquad b_0 = a_0 \frac{sen\alpha_0}{sen\beta_0}, \qquad c_0 = a_0 cos\alpha_0 \left(1 - \frac{tan\alpha_0}{tan\beta_0}\right) \tag{1}$$

The particular case of an elementary square cell corresponds to:

$$l_{0x} = l_{0y} = l \rightarrow \ a_0 cos\alpha_0 = 2a_0 sen\alpha_0 \rightarrow tan\alpha_0 = \frac{1}{2} \tag{2}$$

Due to the discrete nature of the lattice structure, the Poisson's ratio of the elementary cell (with respect to the *x*- and *y*-axis) is defined with respect to a gauge length related to the reference lengths of the cell itself. Therefore, the Poisson's ratio is related to the ratio between the vertical displacements at point B (v_B) and the horizontal one at point A (u_A), namely:

$$\nu = -\frac{\varepsilon_y}{\varepsilon_x}, \qquad \text{with} \quad \varepsilon_x = \frac{u_A}{l_x} \ , \ \ \varepsilon_y = \frac{v_B}{l_y} \tag{3}$$

where l_x, l_y are the reference lengths of the cell, i.e. $l_x = c_0$ in *x*-direction, while $l_y = \frac{l_{0y}}{2}$ in *y*-direction. The deformability of the elementary cell can be determined by introducing some hypotheses that can then be relaxed to get a better accuracy of the model.

In a first attempt, by assuming that the elements of the cell behave as rigid trusses, its motion can be studied through a trivial kinematic analysis under small displacement condition. Accordingly, the Poisson's ratio for an elementary cell is defined as:

$$\nu = -\frac{1}{tan\alpha_0 \ tan\beta_0} \tag{4}$$

that is, it depends only on the geometrical properties of the cell summarised by the two angles α_0, β_0. The variation of the Poisson's ratio as a function of the cell geometry is illustrated in Fig. 2 (note that the relative size of the elememtary cell, defined as the ratio between a reference length and the width of the lattice elements, e.g. a_0/s where s = width of the lattice elements, does not influence these kinematic analysis results). It can be observed that, irrespectively of the angle α_0, the Poisson's ratio is negative for $\beta_0 < 90°$ and tends to unlimited values when $\beta_0 \rightarrow 0°$. It is worth noticing also that Eq. (4) can be applied to a general current configuration of the elementary cell under motion. In such cases, the angles α_0, β_0 have to be regarded as the current inclination angles of the cell elements and the Poisson's ratio as the tangent value related to the tangent displacement vector of the current configuration (note that in this case the reference lengths appearing in Eq. (3) are those related to the current configuration).

Fig. 2. Poisson's ratio vs the inclination angle β_0 for various values of the angle α_0 (for a square cell $\alpha_0 \approx 27°$)

An improvement of the above kinematic approach can be introduced by adopting for the elementary cell a statically indeterminate structural scheme, which accounts for its deformation.

Due to the periodic symmetry conditions arising when several cells are assembled together (see next Section), some rotation constraints can be imposed. The resulting mechanical system can be modelled as a statically undetermined framed structure under a prescribed horizontal displacement at one of its nodes.

The framed structure is characterised by 3 degrees of freedom and the solving system of equations can be written as:

$$\mathbf{K}\cdot\begin{Bmatrix}\mathbf{s}_A\\ \mathbf{s}_B\\ \mathbf{s}_C\end{Bmatrix}=\begin{Bmatrix}\mathbf{Q}_A\\ \mathbf{Q}_B\\ \mathbf{Q}_C\end{Bmatrix} \tag{5a}$$

where $\mathbf{K}$ is the stiffness matrix of the system, $\mathbf{s}_A{}^T=\{u_A \quad 0 \quad 0\}$, $\mathbf{s}_B{}^T=\{u_B \quad v_B \quad 0\}$, $\mathbf{s}_C{}^T=\{0 \quad 0 \quad 0\}$ and $\mathbf{Q}_A,\mathbf{Q}_B,\mathbf{Q}_C$ are the corresponding reaction force vectors.

By writing the stiffness matrix according to the classical Euler-Bernoulli beam formulation, the vector of the unknowns of interest can be explicitly written as:

$$\begin{Bmatrix}u_B\\ v_B\\ Q_{B\varphi}\end{Bmatrix}=\begin{bmatrix}\frac{EA}{a_0}d^2+\frac{12EI}{a_0^3}c^2+\frac{EA}{b_0}f^2+\frac{12EI}{b_0^3}e^2 & \frac{EA}{a_0}cd-\frac{12EI}{a_0^3}cd+\frac{EA}{b_0}ef-\frac{12EI}{b_0^3}ef & 0\\ \frac{EA}{a_0}cd-\frac{12EI}{a_0^3}cd+\frac{EA}{b_0}ef-\frac{12EI}{b_0^3}ef & \frac{EA}{a_0}c^2+\frac{12EI}{a_0^3}d^2+\frac{EA}{b_0}e^2+\frac{12EI}{b_0^3}f^2 & 0\\ \frac{6EI}{a_0^2}c+\frac{6EI}{b_0^2}e & -\frac{6EI}{a_0^2}d-\frac{6EI}{b_0^2}f & 1\end{bmatrix}^{-1}\cdot\begin{Bmatrix}\frac{EA}{b_0}f^2+\frac{12EI}{b_0^3}e^2\\ \frac{EA}{b_0}ef-\frac{12EI}{b_0^3}ef\\ -\frac{6EI}{b_0^2}e\end{Bmatrix}\cdot u_A \tag{5b}$$

where $c=\sin\alpha_0$, $d=\cos\alpha_0$, $e=\sin\beta_0$, $f=\cos\beta_0$, $A=s$ is the area of the beam cross-section, $I=s^3/12$ is the moment of inertial of the beam cross-section (a unit thickness is considered), E is the Young modulus of the material, $Q_{B\varphi}$ is the reaction moment at node B. The ratio v_B/u_A corresponds to the Poisson's ratio of the elementary cell.

By considering a square cell from now onwards ($tan\alpha_0=\frac{1}{2}$), the Poisson's ratio depends only on the angle β_0 and on a relative stiffness parameter defined as $\kappa=K_a/K_b$ (where $K_a=EA/a_0$ and $K_b=EI/a_0^3$), i.e. on the ratio between the axial and the bending stiffness of the beam elements composing the lattice cell.

After some simple but tedious algebraic manipulations, the following expression for the Poisson's ratio of the cell can be obtained:

$$\nu=-\frac{2c_0}{l}\frac{v_B}{u_A}=-(2-\cot\beta_0)\frac{f_I(\beta_0)+\kappa\cdot f_{AI}(\beta_0)+\kappa^2\cdot f_A(\beta_0)}{g_I(\beta_0)+\kappa\cdot g_{AI}(\beta_0)+\kappa^2\cdot g_A(\beta_0)} \tag{6}$$

where $f_I(\beta_0), f_{AI}(\beta_0), f_A(\beta_0), g_I(\beta_0), g_{AI}(\beta_0), g_A(\beta_0)$ are known functions of the inclination angle β_0.

In the case of beam elements constituting the cell with an axial stiffness much greater than the bending one, $\kappa\to\infty$, Eq. (6) reduces to the expression considered in Eq. (4). The above expression (6) can be rewritten by using a relative density parameter ρ_r, defined as the ratio between the bulk density of the material and the theoretical density of the solid phase. Such a parameter can be calculated (with a first order approximation, i.e. by neglecting the overlapped area at the lattice nodes) as the ratio between the area occupied by the material and the whole area of the auxetic cell and it is the complement to unity of the porosity φ, namely

$$\rho_r = \frac{2(a_0 + b_0)}{c_0}\frac{s}{l} = 1 - \varphi \tag{7}$$

The relative stiffness parameter for an elementary cell can be expressed as follows

$$\kappa = \frac{K_a}{K_b} = \frac{A}{I}{a_0}^2 = 12\left(\frac{l}{s\, cos\alpha_0}\right)^2 \tag{8}$$

By manipulating Eq. (7), the relative density ρ_r becomes:

$$\rho_r = \frac{2(a_0 + b_0)}{c_0}\frac{s}{l} = \frac{2\left(1 + \frac{sen\alpha_0}{sen\beta_0}\right)}{cos\alpha_0\left(1 - \frac{tan\beta_0}{tan\beta_0}\right)}\frac{s}{l} \tag{9}$$

By comparing Eq. (8) with Eq. (9), κ can be expressed as a function of ρ_r. Considering the fact that for a square cell $tan\alpha_0 = \frac{1}{2}$, we have

$$\kappa = \frac{T(\beta_0)}{\rho_r^2} \tag{10}$$

where $T(\beta_0)$ is the function of the inclination angle β_0. Finally, by means of Eq. (6) the Poisson's ratio of the square cell can be expressed through the relative density:

$$\boldsymbol{v} = -(2 - cot\beta_0)\cdot\frac{f_I(\beta_0)\cdot\rho_r^4 + f_{AI}(\beta_0)\cdot T(\beta_0)\cdot\rho_r^2 + f_A(\beta_0)\cdot T(\beta_0)^2}{g_I(\beta_0)\cdot\rho_r^4 + g_{AI}(\beta_0)\cdot T(\beta_0)\cdot\rho_r^2 + g_A(\beta_0)\cdot T(\beta_0)^2} \tag{11}$$

The graphical representation of Eq. (11) is illustrated in Fig. 3 where the dependence of the Poisson's ratio on the inclination angle β_0 and on the relative density ρ_r (ranging from 0 to 1) can be observed.

Fig. 3. Poisson's ratio vs the inclination angle β_0 and the relative density ρ_r in the case of a square cell.

Now, by removing the small displacement hypothesis while assuming the cell elements as rigid trusses (kinematic analysis), the cell size and the arrangement of its elements in the current configuration must be considered. The current geometrical features of the cell can be expressed as a function of the lengths a_0, b_0 of the rigid trusses and of the length c which is linearly dependent on the (longitudinal) normal strain along the *x*-axis ε_x:

$$c = c_0(1+\varepsilon_x), \quad \alpha = \arccos\left(\frac{{a_0}^2+c^2-{b_0}^2}{2a_0c}\right), \quad \beta = \arccos\left(-\frac{{b_0}^2+c^2-{a_0}^2}{2b_0c}\right) \tag{12}$$

In the case of large deformation kinematic analysis, the definition of the Poisson's ratio is twofolds, depending on the strain measurement. A nominal (secant) Poisson's ratio can be defined by considering Eq. (3), where the displacement vector joins the reference undeformed configuration with the current one, and the lengths $l_x = c_0$ and $l_y = \frac{l_{0y}}{2}$ are related to the undeformed configuration. Accordingly exploiting Eq. (12), we have:

$$\nu = -\frac{\varepsilon_y}{\varepsilon_x} = \frac{sen\beta - sen\beta_0}{sen\beta_0}\ \frac{c_0}{c-c_0} \tag{13}$$

On the other hand, if one considers in Eq. (3) the tangent displacement vector and the lengths l_x and l_y related to the reference undeformed configuration, the incremental strains $\delta\varepsilon_x$ and $\delta\varepsilon_y$ can in turn be calculated and a tangent Poisson's ratio can be defined (again exploting Eq. (12)):

$$\nu_{tg} = -\frac{\delta\varepsilon_y}{\delta\varepsilon_x} = -\frac{c}{a_0\, sen\alpha}\ \frac{1}{tan\beta - tan\alpha} \tag{14}$$

It is worth noticing that Eq. (14) represents the first derivative of the function $\varepsilon_y = \varepsilon_y(\varepsilon_x)$. If $\varepsilon_x \to 0$ (i.e. for the reference undeformed configuration), nominal and tangent values of the Poisson's ratio coincide and Eq. (14) becomes Eq. (4).

According to the above expression in Fig. 4 the tangent and nominal values of the Poisson's ratio against the longitudinal deformation in *x* direction are plotted for the case of a square cell with $\beta_0 = 50°$.

Fig. 4. Tangent and nominal values of the Poisson's ratio vs the longitudinal deformation for the case of a square cell with $\beta_0 = 50°$.

Finally, by removing all the above simplifying hypotheses, the elementary cell is studied as a framed structure (see Fig. 1b) under a geometrically nonlinear large displacement analysis considering the actual axial and bending stiffness of the cell elements.

Due to the complexity of the above defined problem, a numerical Finite Element (FE) solution can be conveniently adopted. Two-dimensional Euler-Bernoulli beam elements are adopted; geometrically nonlinear analyses are carried out by considering a total Lagrangian element formulation with large displacements and small strains. In Fig. 5 the tangent and nominal values of the Poisson's ratio against the longitudinal deformation in *x* direction are plotted for the case of a square cell with $\beta_0 = 50°$ and different values of the axial-bending relative stiffness parameter κ and the relative density ρ_r.

Fig. 5. Nominal (a) and tangential (b) values of the Poisson's ratio vs the longitudinal deformation for the case of a square cell with $\beta_0 = 50°$ (FE large displacement analysis).

2.2 Assembly of elementary cells

By joining repetitively the elementary cell in both the *x*- and *y*- directions, an auxetic plate can be obtained (Fig. 6) with the same deformation characteristics of the elementary cell itself. Note that the plate is characterized by an orthotropic overall constitutive behaviour, with the material principal axes being aligned with *x*- and *y*-axis. In line with the discussion presented in the previous Section, the Poisson's ratio of the plate corresponding to the ratio between the (transversal) strain ε_y along the *y*-axis and the (longitudinal) strain ε_x along the *x*-axis (ν_{xy} according to the standard notation for orthotropic materials) is studied.

Fig. 6. Assembly of the re-entrant double arrow elementary cells to get an auxetic plate.

Now the geometrical characteristics of the assembled plate can be defined:

$$L_{0x} = mc_0, \qquad L_{0y} = nl_{0y} \tag{15}$$

where *m* and *n* represent the number of cells assembled in the *x*- and *y*-direction, respectively.

Under prescribed relative displacements normal to the two boundaries of the auxetic plate (Δu = relative displacement along the *x*-direction between the points located at $x = b_0 cos\beta_0$ and at $x = L_{xt}$; Δv = relative displacement along the *y*-direction between the points located at $y = 0$ and at $y = L_{0y}$), the nominal deformations of the plate in the *x*- (longitudinal) and *y*- (transversal) directions are given by:

$$\varepsilon_{xt} = \frac{\Delta u}{L_{0x}}, \qquad \varepsilon_{yt} = \frac{\Delta v}{L_{0y}} \tag{16}$$

On the other hand, the longitudinal deformation in the elementary cell is:

$$\varepsilon_x = \frac{u_A}{c_0} = \frac{mu_A}{mc_0} = \frac{\Delta u}{L_{0x}} = \varepsilon_{xt} \tag{17}$$

The total displacement of the plate in the *y*-direction is given by:

$$\Delta v = -n\nu\varepsilon_x l_{0y} = -n\nu\varepsilon_{xt} l_{0y} \tag{18a}$$

and the corresponding deformation

$$\varepsilon_{yt} = -\frac{n\nu\varepsilon_{xt}l_{0y}}{L_{0y}} = -\frac{n\nu\varepsilon_{xt}l_{0y}}{nl_{0y}} = -\nu\varepsilon_{xt} \tag{18b}$$

i.e. the Poisson's coefficient of the plate is the same as that of the elementary cell.

The results shown in Eqs (16)-(18) are strictly valid for an infinite plate, i.e. for a large number of cells along the *x*- and *y*-directions. In the case of finite size plates, the periodicity conditions along the plate boundaries (implying zero rotation about the axis normal to the *xy* plane of the boundary nodes) are not fulfilled. Consequently, the deformed plate presents some non uniform normal displacements along its top and bottom edges (Fig. 7), which might affect the evaluation of the Poisson's ratio according to Eq. (14).

Fig. 7. Auxetic plate subject to a horizontal displacement applied to the right nodes of the assembly: (a) undeformed configuration; (b) deformed configuration; (c) vertical displacements of the nodes of the auxetic plate initially aligned along horizontal lines indicated in (a).

3. Experimental tests

In order to verify the auxetic property of a metamaterial constituted by the assembly of repeated elementary arrow-shaped cells as described above, some experimental tests have been performed on 2-D plates.

3.1 Set up and specimens

A simple mechanical testing machine has been used to study the experimental behaviour of the auxetic sheet under imposed displacements (Fig. 8).

Fig. 8. Experimental testing facility and image of the auxetic plate in its reference undeformed configuration.

The auxetic specimens have been obtained by assembling two different elementary square cells (Fig. 9) that are characterised by a reference length of their edges equal to 20 (sample A) and 15 mm (sample B). The two samples A and B are characterized by a relative density ρ_r (see Eq. (7)) equal to 0.15 and 0.19, respectively. A 3-D printer, based on the so-called FFF technology, is used to produce the specimens made of polylactic acid polymer (PLA). The main features of the printing process are: printing temperature of 196°C, printing speed equal to 35mm/s, thickness of the single printed layer thickness equal to 0.2 mm, nozzle diameter of 0.4 mm.

Fig. 9. Specimens of auxetic plate with elementary square cells (skecthes of the elementary cell and of the assembled plate with details of the gripping system, pictures of the specimens being tested): case of cell length equal to 20 mm, sample A (a), and 15 mm, sample B (b). All dimensions are given in mm.

All the nodes located along the boundary on the right hand side of the plate are subjected to a monotonically increasing longitudinal (along the *x*-direction) displacement measured through a micrometer with a precision 10^{-5} m. A full map of deformed shape of the plate is evaluated through a photographic technique by quantifying the absolute displacements of the nodes of the lattice structure through high resolution pictures taken at given intervals of the applied deformation.

3.2 Results

The deformation maps in the specimens at different deformation steps are obtained on the basis of the nodal displacements measured through photographic technique. In order to get full field maps of displacements from the measured nodal values, bilinear interpolation functions are used. In particular, by considering a regular mesh of four-node finite elements (where each element corresponds to a single elementary cell of the auxetic lattice), Fig. 10, nodal displacements are interpolated through the bilinear shape functions of the elements, , and the strain field in a continuous-like equivalent plate is obtained according to the standard procedure of the finite element method. The nodal displacements are evaluated with respect to their reference undeformed configuration, while an interior region of the plate is adopted for the numerical evaluation of the mean values of the Poisson's ratio (see shaded region in Fig. 10, Tab. 1).

Fig. 10. Scheme of the interior regions adopted for the definition of a mean value of the Poisson's ratio of the sample: sample A (a), and sample B (b).

In Fig. 11 the contour maps of the *x*- and *y*-displacements, and of the corresponding strains, for the sample A are shown. It can be noticed that the displacements field is regular in both the *x*- and *y*-direction, while the strains appear to be not uniform in the considered domain due to small irregularities in the displacements of neighbour nodes. Such irregularities in the strain field are attenuated by increasing the applied deformation.

Fig. 11. Contour maps of the x- and y-displacements (in mm, a, b) and the corresponding strain fields ε_x, ε_y (c, d) for a mean plate longitudinal strain $\varepsilon_x = 5.6\%$ in sample A.

The map of the local values of the Poisson's ratio obtained by using Eq. (3) is presented for different deformation levels; in Fig. 12 the contour map of the Poisson's ratio for the sample A is displayed for an increasing value of the applied longitudinal strain. It can be noted that the Poisson's coefficient tends to attain a nearly uniform distribution inside the plate with a value that is equal to about -0.9.

Fig. 12. Contour maps of the Poisson's ratio for four different levels of the mean plate longitudinal strain ($\varepsilon_x = 2.8\%\ (a), 5.6\%\ (b), 8.5\%\ (c), 14\%\ (d)$) in sample A.

In Fig. 13 the same contour map of the Poisson's ratio for the sample B is displayed for different levels of the applied longitudinal strain; it can be noted that the Poisson's coefficient tends not to attain a nearly uniform distribution inside the plate with a value that is equal to about -1.0.

Fig. 13. Contour maps of the Poisson's ratio for four different levels of the mean plate longitudinal strain ($\varepsilon_x = 3.3\%\ (a), 5.4\%\ (b), 6.3\ (c), 9.7\%\ (d)$) for sample B.

A mean value of the Poisson's ratio (calculated through a weighted average) is summurized in Tab. 1 as a function of the applied longitudinal strain for the two specimens.

Tab. 1. Mean Poisson's ratio for the sample A and B obtained from experiments.

4. Comparison of theoretical and experimental results and discussion

In order to assess for the suitability of FE models for the auxetic plates under study, some geometrically nonlinear numerical analyses are carried out. In order to take into account for the finite size of the nodes of the analysed specimens, a proper rigid link option is introduced in the FE models (Fig. 14a).

Fig. 14. Beam-like model of the of the auxetic cells by considering rigid node features and detail of the rigid parts of the unit cell (a) (dimensions in mm); comparison of the experimental and FE Poisson's ratio for the sample A (b) and B (c) vs the applied longitudinal deformation with and without considering rigid node features in the FE analyses.

As illustrated in Fig. 14b-c and Tab. 2, for both the two samples the average Poisson's ratio obtained from numerical analyses is lower (about 10 to 40%) than the corresponding experimental one, unless the effect of the finite node size is properly accounted for. This correction enables to estimate the Poisson's ratio with a good accuracy compared with the experimentally determined values.

Tab. 2. Average Poisson's ratios for the sample A and B obtained from experiments.

5. Conclusions

So-called metamaterials, i.e. engineered materials having particular and unusual properties obtained thanks to their structure rather than composition, have gained a wide popularity in the last decades. In this context a class of materials known as auxetic are of particular interest due to their negative values of the Poisson's ratio. This enables to produce structural components with, in comparison to traditional couterparts, superior properties (high toughness, resilience, shear resistance, indentation resistance, improved fracture toughness and particular vibration absorption and acoustic properties), which can be exploted in a wide range of applications (biomedical, aerospace, automotive, etc.).

In the present paper a two dimensional auxetic elementary cell, used to generate 2-D sheets by its repetitive assembly, is studied theoretically, experimentally and numerically. The linear and geometrically nonlinear deformability of such auxetic plates is investigated and different approaches to its characterization are critically compared and discussed. Some conclusions related to the relevant potentialities due to the mechanical capability of the auxetic materials in advanced applications involving structural elements, is presented.

References

[1] Baughman, R.H., Dantas S.O., Stafstro, S., Zakhidov, A.A., Mitchell TB., Dubin DHE. (2000). Negative Poisson's ratios for extreme states of matter. Science 288, 2018–2022.

[2] Choi, J.B., Lakes, R.S. (1992). Nonlinear properties of metallic cellular materials with a negative Poisson's ratio. J. Mater. Sci. 27(19), 5373–5381.

[3] Choi, J.B., Lakes, R.S. (1992). Nonlinear properties of polymer cellular materials with a negative Poisson's ratio. J. Mater. Sci. 27(19), 4678–4684.

[4] Scarpa, F., Tomlin, P.J. (2000). On the transverse shear modulus of negative Poisson's ratio honeycomb structures. Fatigue Fract. Eng. Mater. Struct. 23(8), 717–720,

[5] Lakes, R.S., Elms, K.J. (1993). Indentability of conventional and negative Poisson's ratio foams. J. Comp. Mat. 27, 1193–1202.

[6] Choi, J.B., Lakes, R.S. (1996). Fracture toughness of re-entrant foam materials with a negative Poisson's ratio, experiment and analysis. Int. J. Fract. 80, 73–83.

[7] Chen, C.P., Lakes, R.S. (1993). Viscoelastic behaviour of composite-materials with conventional-Poisson-ration or negative-Poisson-ratio foam as one-phase. J. Mater. Sci. 28(16), 4288–4298.

[8] Chen, C.P., Lakes, R.S. (1996). Micromechanical analysis of dynamic behaviour of conventional and negative Poisson's ratio foams. J. Eng. Mater. Technol., ASME 118, 285–288.

[9] Shil'ko, S.V., Petrokovets, E.M., Pleskachevskii, Y.M., (2006). An analysis of contact deformation of auxetic composites. Mech. Comp. Mat. 42(5), 477–484.

[10] Avellanads, M., Swart, P.J. (1998). Calculating the performance of 1-3 piezo composites for hydrophone applications, An effective medium approach. J. Acoust. Soc. Am. 103, 1449–1467.

[11] Friis, E.A., Lakes, R.S., Park, J.B. (1988). Nagative Poisson's ratio polymeric and metallic materials. J. Mater. Sci. 23(12), 4406–4414.

[12] Bhullar, S.K., Hewage, A.T.M., Alderson, A., Alderson, K., Jun, M.B.G. (2013). Influence of negative Poisson's ratio on stent applications. Advances in Materials 2(3), 42–47.

[13] Evans, K.E., Alderson, K.L. (2000). Auxetic materials, the positive side of being negative. Engng. Sci. Edu. J. 9(4), 148–154.

[1] Evans, K.E., Alderson, A. (2000). Auxetic materials, Functional materials and structures from lateral thinking. Adv. Mater. 12(9), 617–628.

[15] Burke, M. (1997). A stretch of the imagination. New Scientist 154(2085), 36–39.

[16] McMullan, P.J. (2004). Textile fibres engineered from molecular auxetic polymers, http,//www.ntcresearch.org/pdf-rpts/AnRp07/M04-GT21-A7.pdf, Accessed Jan. 2015.

[17] Lakes, R.S. (1987). Foam structures with a negative Poisson's ratio. Science 235, 1038–1040.

[18] Lakes, R.S. (1993). Advances in negative Poisson's ratio materials. Adv. Mater. 5, 293–296.

[19] Evans, K.E. (1990). Tailoring the negative Poisson's ratio. Chem. Ind. 20, 654–657.

[20] Stott, P.J., Mitchell, R., Alderson, K., Alderson, A. (2000). A growing industry. Materials World 8, 12–14.

[21] Choi, J.B., Lakes, R.S. (1991). Design of a fastener based on negative Poisson's ratio foam. Cell. Poly. 10, 205–212.

[22] Grima, J.N., Alderson, A., Evans, K.E. (2005). An alternative explanation for the negative Poisson's ratios in auxetic foams. J Phys. Soc. of Japan 74(4), 1341–1342.

[23] Libonati, F., Colombo, C., Vergani, L. Design and characterization of a biomimetic composite inspired to human bone. Fatigue Fract. Eng. Mater. Struct. 37(7), 772–781

[24] Javadi, A.A., Faramarzi, A., Farmani, R. (2012). Design and optimization of microstructure of auxetic materials, Engineering Computations. Int. J. Computer-Aided Engng and Software 29(3), 260–276.

[25] Spagnoli, A., Brighenti, R., Lanfranchi, M., Soncini, F. (2015). On the auxetic behaviour of metamaterials with re-entrant cell structures. Procedia Engineering 109, 410-417.

Nonlinear deformation behaviour of auxetic cellular materials with re-entrant lattice structure

Roberto BRIGHENTI, Andrea SPAGNOLI, Matteo LANFRANCHI, Francesco SONCINI

Department of Civil and Environmental Engineering & Architecture
University of Parma, Parco Area delle Scienze 181/A, 43124 Parma, Italy

** Corresponding author: E-mail: brigh@unipr.it, Phone +39 0521 905910, Fax +39 0521 905924*

Field Code Changed

Abstract

Recent frontiers in material development are represented by ~~the~~ a class of so-called auxetic metamaterials that, ~~having particular and unusual properties~~ thanks to their structure rather than composition, ~~. Among such a wide class of materials the auxetic ones are of particular interest. Auxetic materials~~ are characterised by a negative Poisson's ratio~~, leading to their useful exploitation to a wide range of applications in engineering fields. In particular high fracture toughness, resilience, shear resistance, indentation resistance, and particular vibration absorption and acoustic properties are commonly observed in these classes of solids~~. In the present paper a two dimensional auxetic plate, made by structural straight elements forming a lattice periodic structure with re-entrant cells, is considered. A thorough discussion on the linear and geometrically non-linear deformability of the auxetic plate is presented. The key geometric parameters governing the deformability of the plate are identified and some analytical expressions for calculating the Poisson's ratio, as a function of the applied strain, are given. ~~Theoretical, experimental and~~ N~~n~~umerical (finite element) analyses and experimental tests on 3-D printed specimens are carried out to verify the theoretical findings. For the latter ones, full field strain maps are obtained by means of a suitable interpolation of the sampled displacement field measured by digital image techniques.~~ for the characterisation of its nonlinear deformation properties are presented and compared.~~

Keywords: Metamaterials, Auxetic behaviour, Smart structures, Re-entrant lattice structure.

1. Introduction

So-called metamaterials, obtained through the proper design of their microstructure, can exhibit particular mechanical properties corresponding to a smart behaviour. Among the large class of metamaterials, –auxetic materials – i.e. materials with a negative Poisson's ratio (NPR) – are characterized by an uncommon mechanical behaviour since they show an opposite tendency, with respect to traditional ones: they transversally expand when stretched and contract when compressed[1]. Their behaviour is opposite to those exhibited by the incompressible materials, such as rubbers for which the Poisson's ratio tends to 0.5, and for this reason are also called anti-rubber materials.~~those characterised by negative Poisson's ratio (so-called auxetic property) are of particular interest.~~ Such an uncommon behaviour is usually determined by the material's structure (at the micro or mesoscale) rather than by its composition.

Formatted: Font: 12 pt

Typically the applications where NPR materials are involved, are mainly based on the exploitation of their high toughness, resilience, shear resistance that assume relevant values with respect to others traditional class of solids. In fact auxetic materials are usually characterized by good shear resistance[2-4], indentation resistance[5], noticeable fracture toughness[6], relevant sound and vibration absorption[7,8], high load-carrying capacity due to friction in joints operating under shear loads[9]. It can easily be argued that the negative value of the Poisson's ratio has relevant effects in term of kinematics and deformation of structural elements, and heavily influences the distribution of strains and stresses. As a matter of fact, NPR materials can reduce the stress concentration factor at geometrical discontinuities, enhance the performance of piezoelectric transducers, improve the behaviour of fasteners, bumpers, sound proofing systems and so on[10].

Other relevant applications of NPR materials, are in the biomedical field where the exploitation of the auxetic property is made in the production of hollow pipes for artery opening, obtained by the lateral expansion under tension of such elements and in the mechanical characteristics of surgical implants[11,12]. Suture or muscle/ligament anchors can benefit from these materials as well as for the productions of scaffolds with porous structures, typical of auxetic materials, for tissue regeneration purpose[13,14].

A relevant property of NPR materials can be observed under bending actions: in fact it is well known as traditional materials deform by assuming a configuration that correspond to shrink in the direction perpendicular to the bending plane (anticlastic curvature), while auxetic ones are characterized by an opposite curvature of the edges, i.e. a convex shape occurs (dome-like pattern, occurring in the same direction of the bending force, synclastic curvature). This particular deformation shape can be considered in the design of smart textiles allowing to follow the synclastic double curvatures of the human body, and enables to produce elements which easily conform to shapes normally required in the automotive and aerospace industries[15-16].

More traditional engineering applications can also have relevant advantages from the use of NPR materials: fibre reinforced composites with auxetic reinforcement (auxetic fibres easily resist to pull-out thanks to the expansion when stretched), smart fasteners and rivets, structural elements with high impact and indentation strength, high shock and sound energy absorption[17-21], fasteners and tuneable filters, materials for high technology packing, knee and elbow pads, etc.

A relevant aspect concerning the NPR materials is that, typically, their auxeticity does not depend on the size scale of the structural component, leading to the possibility to design auxetic “expandable” elements, usefully adopted to realize space structures such as antennas and shields: they have a compact shape and self-contained volume until they “open up” when tensioned in their final destination place[22].

It is worth mention that the design and production of materials having these unusual properties is nowadays possible; materials with NPR property, such as microporous polymers, metallic foams, auxetic fibres and rivets, paper sheets, natural materials (such as bone, e.g. see Ref. 23), in the last decades have been recognized, designed or produced[24].

~~Auxetic materials have for instance been employed for the development of smart structures – enabling the optimization and self tuning of the response of engineering systems on the basis of the applied actions[1]. Typical smart structures are represented by sensing structures, adaptive structural elements, devices employing auto-adaptive capabilities (as shape memory alloys, SMA, piezoelectric materials, PZT, magneto-rheological, MR, and electro-rheological, ER, fluids), materials with self-repairing capabilities (self-healing, SH), etc. Smart structures are currently employed in applications where an active control is required such as vibration (AVC), active noise control (ANC), active shape control (ASC), active health monitoring (AHM), industrial and biomechanical issues, and so on.~~

~~Smart structures and systems provide a feedback control of their mechanical response, on one hand by determining the current status of the element through sensors and on the other hand by using actuators to modify and adapt the configuration of the element according to some desired requirements. Both sensors (such as strain gauges, optical fibres, piezoelectric sensors, thermistors, thermocouples) and actuators (such as shape memory alloys, magnetostrictive materials, piezoelectric materials) are usually incorporated into the structural element.~~

~~In this context, the auxetic materials can usefully be adopted to obtain particular structural response, capable of performing an optimum behaviour under external actions. Such uncommon behaviour is usually obtained by metamaterials, namely engineered materials that exhibit particular~~

~~and unusual properties thanks to their structure rather than composition (note that some examples of metamaterials exhibiting auxetic behaviour can also be found in nature).~~

In the present paper a brief introduction on auxetic materials is presented by underlying their potentiality in the design of structural elements. Then, a metamaterial plate, obtained by assembling elementary auxetic cells with different geometrical parameters, is considered: both ~~experimental and~~ numerical analyses and experimental tests are performed on such an auxetic sheet and the results are compared. A thourough discussion about the obtained structural response in terms of linear and geometrically nonlinear deformability is given. Some preliminary results have been presented in Ref. 25.

~~**2. Some mechanical issues of auxetic materials and their smart applications**~~

~~Auxetic materials – i.e. materials with a negative Poisson's ratio (NPR) – are characterized by an uncommon mechanical behaviour since they show an opposite tendency, with respect to traditional ones: they transversally expand when stretched and contract when compressed[1]. Their behaviour is opposite to those exhibited by the incompressible materials, such as rubbers for which the Poisson's ratio tends to 0.5, and for this reason are also called anti-rubber materials.~~

~~Typically the applications where NPR materials are involved, are mainly based on the exploitation of their high toughness, resilience, shear resistance that assume relevant values with respect to others traditional class of solids. In fact auxetic materials are usually characterized by good shear resistance[2-4], indentation resistance[5], noticeable fracture toughness[6], relevant sound and vibration absorption[7,8], high load carrying capacity due to friction in joints operating under shear loads[9]. It can easily be argued that the negative value of the Poisson's ratio has relevant effects in term of kinematics and deformation of structural elements, and heavily influences the distribution of strains and stresses. As a matter of fact, NPR materials can reduce the stress concentration factor at geometrical discontinuities, enhance the performance of piezoelectric transducers, improve the behaviour of fasteners, bumpers, sound proofing systems and so on[10].~~

~~Other relevant applications of NPR materials, are in the biomedical field where the exploitation of the auxetic property is made in the production of hollow pipes for artery opening, obtained by the lateral expansion under tension of such elements and in the mechanical characteristics of surgical implants[11,12]. Suture or muscle/ligament anchors can benefit from these materials as well as for the productions of scaffolds with porous structures, typical of auxetic materials, for tissue regeneration purpose[13,14].~~

~~A relevant property of NPR materials can be observed under bending actions: in fact it is well known as traditional materials deform by assuming a configuration that correspond to shrink in the~~

~~direction perpendicular to the bending plane (anticlastic curvature), while auxetic ones are characterized by an opposite curvature of the edges, i.e. a convex shape occurs (dome-like pattern, occurring in the same direction of the bending force, synclastic curvature). This particular deformation shape can be considered in the design of smart textiles allowing to follow the synclastic double curvatures of the human body, and enables to produce elements which easily conform to shapes normally required in the automotive and aerospace industries[15-18].~~

~~More traditional engineering applications can also have relevant advantages from the use of NPR materials: fibre reinforced composites with auxetic reinforcement (auxetic fibres easily resist to pull-out thanks to the expansion when stretched), smart fasteners and rivets, structural elements with high impact and indentation strength, high shock and sound energy absorption[19-21], fasteners and tuneable filters, materials for high technology packing, knee and elbow pads, etc.~~

~~A relevant aspect concerning the NPR materials is that, typically, their auxeticity does not depend on the size scale of the structural component, leading to the possibility to design auxetic "expandable" elements, usefully adopted to realize space structures such as antennas and shields: they have a compact shape and self-contained volume until they "open up" when tensioned in their final destination place[22].~~

~~It is worth mention that the design and production of materials having these unusual properties is nowadays possible; materials with NPR property, such as microporous polymers, metallic foams, auxetic fibres and rivets, paper sheets, natural materials (such as bone, e.g. see Ref. 23), in the last decades have been recognized, designed or produced[24].~~

2~~3~~. An auxetic material with re-entrant lattice structure

In the present study a lattice-like 2-D auxetic sheet is considered; its unit cell is characterised by a re-entrant double arrow shape as shown in Fig. 1.

Fig. 1. Geometrical characteristics of the elementary auxetic cell (a). Structural scheme of the cell (b).

2~~3~~.1 Mechanical modeling of the elementary cell

The geometrical properties of the elementary cell are defined by three parameters, e.g. the reference length a_0 and the two angles α_0, β_0 . On the basis of these three geometrical parameters, all the relevant dimensions of the cell can be deduced:

$$l_{0x} = a_0 cos\alpha_0, \qquad l_{0y} = 2a_0 sen\alpha_0, \qquad b_0 = a_0 \frac{sen\alpha_0}{sen\beta_0}, \qquad c_0 = a_0 cos\alpha_0 \left(1 - \frac{tan\alpha_0}{tan\beta_0}\right) \tag{1}$$

The particular case of an elementary square cell corresponds to:

$$l_{0x} = l_{0y} = l \rightarrow \ a_0 cos\alpha_0 = 2a_0 sen\alpha_0 \rightarrow tan\alpha_0 = \frac{1}{2} \tag{2}$$

Due to the discrete nature of the lattice structure, the Poisson's ratio of the elementary cell (with respect to the *x*- and *y*-axis) is defined with respect to a gauge length related to the reference lengths of the cell itself. Therefore, the Poisson's ratio is related to the ratio between the vertical displacements at point B (v_B) and the horizontal one at point A (u_A), namely:

$$\nu = -\frac{\varepsilon_y}{\varepsilon_x}, \qquad \text{with} \quad \varepsilon_x = \frac{u_A}{l_x} \ , \ \ \varepsilon_y = \frac{v_B}{l_y} \tag{3}$$

where l_x, l_y are the reference lengths of the cell, i.e. $l_x = c_0$ in *x*-direction, while $l_y = \frac{l_{0y}}{2}$ in *y*-direction. The deformability of the elementary cell can be determined by introducing some hypotheses that can then be relaxed to get a better accuracy of the model.

In a first attempt, by assuming that the elements of the cell behave as rigid trusses, its motion can be studied through a trivial kinematic analysis under small displacement condition. Accordingly, the Poisson's ratio for an elementary cell is defined as:

$$\nu = -\frac{1}{tan\alpha_0 \ tan\beta_0} \tag{4}$$

that is, it depends only on the geometrical properties of the cell summarised by the two angles α_0, β_0. The variation of the Poisson's ratio as a function of the cell geometry is illustrated in Fig. 2 (note that the relative size of the elememtary cell, defined as the ratio between a reference length and the width of the lattice elements, e.g. a_0/s where s = width of the lattice elements, does not influence these kinematic analysis results). It can be observed that, irrespectively of the angle α_0, the Poisson's ratio is negative for $\beta_0 < 90°$ and tends to unlimited values when $\beta_0 \rightarrow 0°$. It is worth noticing also that Eq. (4) can be applied to a general current configuration of the elementary cell under motion. In such cases, the angles α_0, β_0 have to be regarded as the current inclination angles of the cell elements and the Poisson's ratio as the tangent value related to the tangent displacement vector of the current configuration (note that in this case the reference lengths appearing in Eq. (3) are those related to the current configuration).

Fig. 2. Poisson's ratio vs the inclination angle β_0 for various values of the angle α_0 (for a square cell $\alpha_0 \approx 27°$)

An improvement of the above kinematic approach can be introduced by adopting for the elementary cell a statically indeterminate structural scheme, which accounts for its deformation. Due to the periodic symmetry conditions arising when several cells are assembled together (see next Section), some rotation constraints can be imposed. The resulting mechanical system can be modelled as a statically undetermined framed structure under a prescribed horizontal displacement at one of its nodes.

The framed structure is characterised by 3 degrees of freedom and the solving system of equations can be written as:

$$\mathbf{K}\cdot\begin{Bmatrix}\mathbf{s}_A\\ \mathbf{s}_B\\ \mathbf{s}_C\end{Bmatrix}=\begin{Bmatrix}\mathbf{Q}_A\\ \mathbf{Q}_B\\ \mathbf{Q}_C\end{Bmatrix} \tag{5a}$$

where $\mathbf{K}$ is the stiffness matrix of the system, ${\mathbf{s}_A}^T=\{u_A \quad 0 \quad 0\}$, ${\mathbf{s}_B}^T=\{u_B \quad v_B \quad 0\}$, ${\mathbf{s}_C}^T=\{0 \quad 0 \quad 0\}$ and $\mathbf{Q}_A, \mathbf{Q}_B, \mathbf{Q}_C$ are the corresponding reaction force vectors.

By writing the stiffness matrix according to the classical Euler-Bernoulli beam formulation, the vector of the unknowns of interest can be explicitly written as:

$$\begin{Bmatrix}u_B\\ v_B\\ Q_{B\varphi}\end{Bmatrix}=\begin{bmatrix}\frac{EA}{a_0}d^2+\frac{12EI}{{a_0}^3}c^2+\frac{EA}{b_0}f^2+\frac{12EI}{{b_0}^3}e^2 & \frac{EA}{a_0}cd-\frac{12EI}{{a_0}^3}cd+\frac{EA}{b_0}ef-\frac{12EI}{{b_0}^3}ef & 0\\ \frac{EA}{a_0}cd-\frac{12EI}{{a_0}^3}cd+\frac{EA}{b_0}ef-\frac{12EI}{{b_0}^3}ef & \frac{EA}{a_0}c^2+\frac{12EI}{{a_0}^3}d^2+\frac{EA}{b_0}e^2+\frac{12EI}{{b_0}^3}f^2 & 0\\ \frac{6EI}{{a_0}^2}c+\frac{6EI}{{b_0}^2}e & -\frac{6EI}{{a_0}^2}d-\frac{6EI}{{b_0}^2}f & 1\end{bmatrix}^{-1}\cdot\begin{Bmatrix}\frac{EA}{b_0}f^2+\frac{12EI}{{b_0}^3}e^2\\ \frac{EA}{b_0}ef-\frac{12EI}{{b_0}^3}ef\\ -\frac{6EI}{{b_0}^2}e\end{Bmatrix}\cdot u_A \tag{5b}$$

where $c=\sin\alpha_0$, $d=\cos\alpha_0$, $e=\sin\beta_0$, $f=\cos\beta_0$, $A=s$ is the area of the beam cross-section, $I=s^3/12$ is the moment of inertial of the beam cross-section (a unit thickness is considered), E is the Young modulus of the material, $Q_{B\varphi}$ is the reaction moment at node B. The ratio v_B/u_A corresponds to the Poisson's ratio of the elementary cell.

By considering a square cell from now onwards ($tan\alpha_0=\frac{1}{2}$), the Poisson's ratio depends only on the angle β_0 and on a relative stiffness parameter defined as $\kappa=K_a/K_b$ (where $K_a=EA/a_0$ and $K_b=EI/a_0^3$), i.e. on the ratio between the axial and the bending stiffness of the beam elements composing the lattice cell.

After some simple but tedious algebraic manipulations, the following expression for the Poisson's ratio of the cell can be obtained:

$$\nu=-\frac{2c_0}{l}\frac{v_B}{u_A}=-(2-\cot\beta_0)\frac{f_I(\beta_0)+\kappa\cdot f_{AI}(\beta_0)+\kappa^2\cdot f_A(\beta_0)}{g_I(\beta_0)+\kappa\cdot g_{AI}(\beta_0)+\kappa^2\cdot g_A(\beta_0)} \tag{6}$$

where $f_I(\beta_0), f_{AI}(\beta_0), f_A(\beta_0), g_I(\beta_0), g_{AI}(\beta_0), g_A(\beta_0)$ are known functions of the inclination angle β_0.

In the case of beam elements constituting the cell with an axial stiffness much greater than the bending one, $\kappa \to \infty$, Eq. (6) reduces to the expression considered in Eq. (4). The above expression (6) can be rewritten by using a relative density parameter ρ_r, defined as the ratio between the bulk density of the material and the theoretical density of the solid phase. Such a parameter can be calculated (with a first order approximation, i.e. by neglecting the overlapped area at the lattice nodes) as the ratio between the area occupied by the material and the whole area of the auxetic cell and it is the complement to unity of the porosity φ, namely

$$\rho_r = \frac{2(a_0 + b_0)}{c_0}\frac{s}{l} = 1 - \varphi \tag{7}$$

The relative stiffness parameter for an elementary cell can be expressed as follows

$$\kappa = \frac{K_a}{K_b} = \frac{A}{I}{a_0}^2 = 12\left(\frac{l}{s\,cos\alpha_0}\right)^2 \tag{8}$$

By manipulating Eq. (7), the relative density ρ_r becomes:

$$\rho_r = \frac{2(a_0 + b_0)}{c_0}\frac{s}{l} = \frac{2\left(1 + \frac{sen\alpha_0}{sen\beta_0}\right)}{cos\alpha_0\left(1 - \frac{tan\beta_0}{tan\beta_0}\right)}\frac{s}{l} \tag{9}$$

By comparing Eq. (8) with Eq. (9), κ can be expressed as a function of ρ_r. Considering the fact that for a square cell $tan\alpha_0 = \frac{1}{2}$, we have

$$\kappa = \frac{T(\beta_0)}{\rho_r^2} \tag{10}$$

where $T(\beta_0)$ is the function of the inclination angle β_0. Finally, by means of Eq. (6) the Poisson's ratio of the square cell can be expressed through the relative density:

$$\boldsymbol{v} = -(2 - cot\beta_0) \cdot \frac{f_I(\beta_0) \cdot \rho_r^4 + f_{AI}(\beta_0) \cdot T(\beta_0) \cdot \rho_r^2 + f_A(\beta_0) \cdot T(\beta_0)^2}{g_I(\beta_0) \cdot \rho_r^4 + g_{AI}(\beta_0) \cdot T(\beta_0) \cdot \rho_r^2 + g_A(\beta_0) \cdot T(\beta_0)^2} \tag{11}$$

The graphical representation of Eq. (11) is illustrated in Fig. 3 where the dependence of the Poisson's ratio on the inclination angle β_0 and on the relative density ρ_r (ranging from 0 to 1) can be observed.

Fig. 3. Poisson's ratio vs the inclination angle β_0 and the relative density ρ_r in the case of a square cell.

Now, by removing the small displacement hypothesis while assuming the cell elements as rigid trusses (kinematic analysis), the cell size and the arrangement of its elements in the current configuration must be considered. The current geometrical features of the cell can be expressed as a function of the lengths a_0, b_0 of the rigid trusses and of the length c which is linearly dependent on the (longitudinal) normal strain along the *x*-axis ε_x:

$$c = c_0(1+\varepsilon_x), \quad \alpha = \arccos\left(\frac{{a_0}^2+c^2-{b_0}^2}{2a_0 c}\right), \quad \beta = \arccos\left(-\frac{{b_0}^2+c^2-{a_0}^2}{2b_0 c}\right) \tag{12}$$

In the case of large deformation kinematic analysis, the definition of the Poisson's ratio is twofolds, depending on the strain measurement. A nominal (secant) Poisson's ratio can be defined by considering Eq. (3), where the displacement vector joins the reference undeformed configuration with the current one, and the lengths $l_x = c_0$ and $l_y = \frac{l_{0y}}{2}$ are related to the undeformed configuration. Accordingly exploiting Eq. (12), we have:

$$\nu = -\frac{\varepsilon_y}{\varepsilon_x} = \frac{sen\beta - sen\beta_0}{sen\beta_0} \; \frac{c_0}{c-c_0} \tag{13}$$

On the other hand, if one considers in Eq. (3) the tangent displacement vector and the lengths l_x and l_y related to the reference undeformed configuration, the incremental strains $\delta\varepsilon_x$ and $\delta\varepsilon_y$ can in turn be calculated and a tangent Poisson's ratio can be defined (again exploting Eq. (12)):

$$\nu_{tg} = -\frac{\delta\varepsilon_y}{\delta\varepsilon_x} = -\frac{c}{a_0\, sen\alpha} \; \frac{1}{tan\beta - tan\alpha} \tag{14}$$

It is worth noticing that Eq. (14) represents the first derivative of the function $\varepsilon_y = \varepsilon_y(\varepsilon_x)$. If $\varepsilon_x \to 0$ (i.e. for the reference undeformed configuration), nominal and tangent values of the Poisson's ratio coincide and Eq. (14) becomes Eq. (4).

According to the above expression in Fig. 4 the tangent and nominal values of the Poisson's ratio against the longitudinal deformation in *x* direction are plotted for the case of a square cell with $\beta_0 = 50°$.

Fig. 4. Tangent and nominal values of the Poisson's ratio vs the longitudinal deformation for the case of a square cell with $\beta_0 = 50°$.

Finally, by removing all the above simplifying hypotheses, the elementary cell is studied as a framed structure (see Fig. 1b) under a geometrically nonlinear large displacement analysis considering the actual axial and bending stiffness of the cell elements.

Due to the complexity of the above defined problem, a numerical Finite Element (FE) solution can be conveniently adopted. Two-dimensional Euler-Bernoulli beam elements are adopted; geometrically nonlinear analyses are carried out by considering a total Lagrangian element formulation with large displacements and small strains. In Fig. 5 the tangent and nominal values of the Poisson's ratio against the longitudinal deformation in x direction are plotted for the case of a square cell with $\beta_0 = 50°$ and different values of the axial-bending relative stiffness parameter κ and the relative density ρ_r.

Fig. 5. Nominal (a) and tangential (b) values of the Poisson's ratio vs the longitudinal deformation for the case of a square cell with $\beta_0 = 50°$ (FE large displacement analysis).

2~~3~~.2 Assembly of elementary cells

By joining repetitively the elementary cell in both the x- and y- directions, an auxetic plate can be obtained (Fig. 6) with the same deformation characteristics of the elementary cell itself. Note that the plate is characterized by an orthotropic overall constitutive behaviour, with the material principal axes being aligned with x- and y-axis. In line with the discussion presented in the previous Section, the Poisson's ratio of the plate corresponding to the ratio between the (transversal) strain ε_y along the y-axis and the (longitudinal) strain ε_x along the x-axis (ν_{xy} according to the standard notation for orthotropic materials) is studied.

Fig. 6. Assembly of the re-entrant double arrow elementary cells to get an auxetic plate.

Now the geometrical characteristics of the assembled plate can be defined:

$$L_{0x} = mc_0, \qquad L_{0y} = nl_{0y} \tag{15}$$

where m and n represent the number of cells assembled in the x- and y-direction, respectively.

Under prescribed relative displacements normal to the two boundaries of the auxetic plate (Δu = relative displacement along the x-direction between the points located at $x = b_0 cos\beta_0$ and at $x = L_{xt}$; Δv = relative displacement along the y-direction between the points located at $y = 0$ and at $y = L_{0y}$), the nominal deformations of the plate in the x- (longitudinal) and y- (transversal) directions are given by:

$$\varepsilon_{xt} = \frac{\Delta u}{L_{0x}}, \qquad \varepsilon_{yt} = \frac{\Delta v}{L_{0y}} \tag{16}$$

On the other hand, the longitudinal deformation in the elementary cell is:

$$\varepsilon_x = \frac{u_A}{c_0} = \frac{mu_A}{mc_0} = \frac{\Delta u}{L_{0x}} = \varepsilon_{xt} \tag{17}$$

The total displacement of the plate in the *y*-direction is given by:

$$\Delta v = -n\nu\varepsilon_x l_{0y} = -n\nu\varepsilon_{xt} l_{0y} \tag{18a}$$

and the corresponding deformation

$$\varepsilon_{yt} = -\frac{n\nu\varepsilon_{xt} l_{0y}}{L_{0y}} = -\frac{n\nu\varepsilon_{xt} l_{0y}}{n l_{0y}} = -\nu\varepsilon_{xt} \tag{18b}$$

i.e. the Poisson's coefficient of the plate is the same as that of the elementary cell.

The results shown in Eqs (16)-(18) are strictly valid for an infinite plate, i.e. for a large number of cells along the *x*- and *y*-directions. In the case of finite size plates, the periodicity conditions along the plate boundaries (implying zero rotation about the axis normal to the *xy* plane of the boundary nodes) are not fulfilled. Consequently, the deformed plate presents some non uniform normal displacements along its top and bottom edges (Fig. 7), which might affect the evaluation of the Poisson's ratio according to Eq. (14).

Fig. 7. Auxetic plate subject to a horizontal displacement applied to the right nodes of the assembly: (a) undeformed configuration; (b) deformed configuration; (c) vertical displacements of the nodes of the auxetic plate initially aligned along horizontal lines indicated in (a).

~~3~~4. Experimental tests

In order to verify the auxetic property of a metamaterial constituted by the assembly of repeated elementary arrow-shaped cells as described above, some experimental tests have been performed on 2-D plates.

~~4~~3.1 Set up and specimens

A simple mechanical testing machine has been used to study the experimental behaviour of the auxetic sheet under imposed displacements (Fig. 8).

Fig. 8. Experimental testing facility and image of the auxetic plate in its reference undeformed configuration.

The auxetic specimens have been obtained by assembling two different elementary square cells (Fig. 9) that are characterised by a reference length of their edges equal to 20 (sample A) and 15 mm (sample B). The two samples A and B are characterized by a relative density ρ_r (see Eq. (7)) equal to 0.15 and 0.19, respectively. A 3-D printer, based on the so-called FFF technology, is used to produce the specimens made of polylactic acid polymer (PLA). The main features of the printing process are: printing temperature of 196°C, printing speed equal to 35mm/s, thickness of the single printed layer thickness equal to 0.2 mm, nozzle diameter of 0.4 mm.

Fig. 9. Specimens of auxetic plate with elementary square cells (skecthes of the elementary cell and of the assembled plate with details of the gripping system, pictures of the specimens being tested): case of cell length equal to 20 mm, sample A (a), and 15 mm, sample B (b). All dimensions are given in mm.

All the nodes located along the boundary on the right hand side of the plate are subjected to a monotonically increasing longitudinal (along the *x*-direction) displacement measured through a micrometer with a precision 10^{-5} m. A full map of deformed shape of the plate is evaluated through a photographic technique by quantifying the absolute displacements of the nodes of the lattice structure through high resolution pictures taken at given intervals of the applied deformation.

~~4~~3.2 Results

The deformation maps in the specimens at different deformation steps are obtained on the basis of the nodal displacements measured through photographic technique. In order to get full field maps of displacements from the measured nodal values, bilinear interpolation functions are used. In particular, by considering a regular mesh of four-node finite elements (where each element corresponds to a single elementary cell of the auxetic lattice), Fig. 10, ~~Such~~ nodal displacements are interpolated through the~~classical~~ bilinear shape functions of the elements, ~~referred to a background rectangular cell framework (Fig. 10)~~, and~~in order to get~~ the strain field in a continuous-like equivalent plate is obtained according to the standard procedure of the finite element method. The nodal displacements are evaluated with respect to their reference undeformed configuration, while an interior region of the plate is adopted for the numerical evaluation of the mean values of the Poisson's ratio (see shaded region in Fig. 10, Tab. 1).

Fig. 10. Scheme of the interior regions adopted for the definition of a mean value of the Poisson's ratio of the sample: sample A (a), and sample B (b).

In Fig. 11 the contour maps of the *x*- and *y*-displacements, and of the corresponding strains, for the sample A are shown. It can be noticed that the displacements field is regular in both the *x*- and *y*-direction, while the strains appear to be not uniform in the considered domain due to small irregularities in the displacements of neighbour nodes. Such irregularities in the strain field are attenuated by increasing the applied deformation.

Fig. 11. Contour maps of the x- and y-displacements (in mm, a, b) and the corresponding strain fields ε_x, ε_y (c, d) for a mean plate longitudinal strain $\varepsilon_x = 5.6\%$ in sample A.

The map of the local values of the Poisson's ratio obtained by using Eq. (3) is presented for different deformation levels; in Fig. 12 the contour map of the Poisson's ratio for the sample A is displayed for an increasing value of the applied longitudinal strain. It can be noted that the Poisson's coefficient tends to attain a nearly uniform distribution inside the plate with a value that is equal to about -0.9.

Fig. 12. Contour maps of the Poisson's ratio for four different levels of the mean plate longitudinal strain ($\varepsilon_x = 2.8\%\ (a), 5.6\%\ (b), 8.5\%\ (c), 14\%\ (d)$) in sample A.

In Fig. 13 the same contour map of the Poisson's ratio for the sample B is displayed for different levels of the applied longitudinal strain; it can be noted that the Poisson's coefficient tends not to attain a nearly uniform distribution inside the plate with a value that is equal to about -1.0.

Fig. 13. Contour maps of the Poisson's ratio for four different levels of the mean plate longitudinal strain ($\varepsilon_x = 3.3\%\ (a), 5.4\%\ (b), 6.3\ (c), 9.7\%\ (d)$) for sample B.

A mean value of the Poisson's ratio (calculated through a weighted average) is summurized in Tab. 1 as a function of the applied longitudinal strain for the two specimens.

Tab. 1. Mean Poisson's ratio for the sample A and B obtained from experiments.

4~~5~~. Comparison of theoretical and experimental results and discussion

In order to assess for the suitability of FE models for the auxetic plates under study, some geometrically nonlinear numerical analyses are carried out. In order to take into account for the finite size of the nodes of the analysed specimens, a proper rigid link option is introduced in the FE models (Fig. 14a).

Fig. 14. Beam-like model of the of the auxetic cells by considering rigid node features and detail of the rigid parts of the unit cell (a) (dimensions in mm); comparison of the experimental and FE Poisson's ratio for the sample A (b) and B (c) vs the applied longitudinal deformation with and without considering rigid node features in the FE analyses.

As illustrated in Fig. 14b-c and Tab. 2, for both the two samples the average Poisson's ratio obtained from numerical analyses is lower (about 10 to 40%) than the corresponding experimental one, unless the effect of the finite node size is properly accounted for. This correction enables to estimate the Poisson's ratio with a good accuracy compared with the experimentally determined values.

Tab. 2. Average Poisson's ratios for the sample A and B obtained from experiments.

5~~6~~. Conclusions

So-called metamaterials, i.e. engineered materials having particular and unusual properties obtained thanks to their structure rather than composition, have gained a wide popularity in the last decades. In this context a class of materials known as auxetic are of particular interest due to their negative values of the Poisson's ratio. This enables to produce structural components with, in comparison to traditional couterparts, superior properties (high toughness, resilience, shear resistance, indentation resistance, improved fracture toughness and particular vibration absorption and acoustic properties), which can be exploted in a wide range of applications (biomedical, aerospace, automotive, etc.).

In the present paper a two dimensional auxetic elementary cell, used to generate 2-D sheets by its repetitive assembly, is studied theoretically, experimentally and numerically. The linear and geometrically nonlinear deformability of such auxetic plates is investigated and different approaches to its characterization are critically compared and discussed. Some conclusions related to the relevant potentialities due to the mechanical capability of the auxetic materials in advanced applications involving structural elements, is presented.

References

[1] Baughman, R.H., Dantas S.O., Stafstro, S., Zakhidov, A.A., Mitchell TB., Dubin DHE. (2000). Negative Poisson's ratios for extreme states of matter. Science 288, 2018–2022.

[2] Choi, J.B., Lakes, R.S. (1992). Nonlinear properties of metallic cellular materials with a negative Poisson's ratio. J. Mater. Sci. 27(19), 5373–5381.

[3] Choi, J.B., Lakes, R.S. (1992). Nonlinear properties of polymer cellular materials with a negative Poisson's ratio. J. Mater. Sci. 27(19), 4678–4684.

[4] Scarpa, F., Tomlin, P.J. (2000). On the transverse shear modulus of negative Poisson's ratio honeycomb structures. Fatigue~~.~~ Fract. Eng.~~ng~~ Mater. ~~&~~ Struct. 23(8), 717–720,

[5] Lakes, R.S., Elms, K.J. (1993). Indentability of conventional and negative Poisson's ratio foams. J. Comp. Mat. 27, 1193–1202.

[6] Choi, J.B., Lakes, R.S. (1996). Fracture toughness of re-entrant foam materials with a negative Poisson's ratio, experiment and analysis. Int. J. Fract. 80, 73–83.

[7] Chen, C.P., Lakes, R.S. (1993). Viscoelastic behaviour of composite-materials with conventional-Poisson-ration or negative-Poisson-ratio foam as one-phase. J. Mater. Sci. 28(16), 4288–4298.

[8] Chen, C.P., Lakes, R.S. (1996). Micromechanical analysis of dynamic behaviour of conventional and negative Poisson's ratio foams. J. Eng. Mater. Technol., ASME 118, 285–288.

[9] Shil'ko, S.V., Petrokovets, E.M., Pleskachevskii, Y.M., (2006). An analysis of contact deformation of auxetic composites. Mech. Comp. Mat. 42(5), 477–484.

[10] Avellanads, M., Swart, P.J. (1998). Calculating the performance of 1-3 piezo composites for hydrophone applications, An effective medium approach. J. Acoust. Soc. Am. 103, 1449–1467.

[11] Friis, E.A., Lakes, R.S., Park, J.B. (1988). Nagative Poisson's ratio polymeric and metallic materials. J. Mater. Sci. 23(12), 4406–4414.

[12] Bhullar, S.K., Hewage, A.T.M., Alderson, A., Alderson, K., Jun, M.B.G. (2013). Influence of negative Poisson's ratio on stent applications. Advances in Materials 2(3), 42–47.

[13] Evans, K.E., Alderson, K.L. (2000). Auxetic materials, the positive side of being negative. Engng. Sci. Edu. J. 9(4), 148–154.

[1] Evans, K.E., Alderson, A. (2000). Auxetic materials, Functional materials and structures from lateral thinking. Adv. Mater. 12(9), 617–628.

[15] Burke, M. (1997). A stretch of the imagination. New Scientist 154(2085), 36–39.

[16] McMullan, P.J. (2004). Textile fibres engineered from molecular auxetic polymers, http,//www.ntcresearch.org/pdf-rpts/AnRp07/M04-GT21-A7.pdf, Accessed Jan. 2015.

[17] Lakes, R.S. (1987). Foam structures with a negative Poisson's ratio. Science 235, 1038–1040.

[18] Lakes, R.S. (1993). Advances in negative Poisson's ratio materials. Adv. Mater. 5, 293–296.

[19] Evans, K.E. (1990). Tailoring the negative Poisson's ratio. Chem. Ind. 20, 654–657.

[20] Stott, P.J., Mitchell, R., Alderson, K., Alderson, A. (2000). A growing industry. Materials World 8, 12–14.

[21] Choi, J.B., Lakes, R.S. (1991). Design of a fastener based on negative Poisson's ratio foam. Cell. Poly. 10, 205–212.

Field Code Changed

[22] Grima, J.N., Alderson, A., Evans, K.E. (2005). An alternative explanation for the negative Poisson's ratios in auxetic foams. J Phys. Soc. of Japan 74(4), 1341–1342.

[23] Libonati, F., Colombo, C., Vergani, L. Design and characterization of a biomimetic composite inspired to human bone. Fatigue~~.~~ Fract. Eng.~~ng~~ Mater. ~~&~~ Struct. 37(7), 772–781

[24] Javadi, A.A., Faramarzi, A., Farmani, R. (2012). Design and optimization of microstructure of auxetic materials, Engineering Computations. Int. J. Computer-Aided Engng and Software 29(3), 260–276.

[25] Spagnoli, A., Brighenti, R., Lanfranchi, M., Soncini, F. (2015). On the auxetic behaviour of metamaterials with re-entrant cell structures. Procedia Engineering 109, 410-417.

Formatted: English (U.S.)

Formatted: English (U.S.)

Field Code Changed

FIGURE AND TABLE CAPTIONS

Fig. 1. Geometrical characteristics of the elementary auxetic cell (a). Structural scheme of the cell (b).

Fig. 2. Poisson's ratio vs the inclination angle β_0 for various values of the angle α_0 (for a square cell $\alpha_0 \approx 27°$)

Fig. 3. Poisson's ratio vs the inclination angle β_0 and the relative density ρ_r in the case of a square cell.

Fig. 4. Tangent and nominal values of the Poisson's ratio vs the longitudinal deformation for the case of a square cell with $\beta_0 = 50°$.

Fig. 5. Nominal (a) and tangential (b) values of the Poisson's ratio vs the longitudinal deformation for the case of a square cell with $\beta_0 = 50°$ (FE large displacement analysis).

Fig. 6. Assembly of the re-entrant double arrow elementary cells to get an auxetic plate.

Fig. 7. Auxetic plate subject to a horizontal displacement applied to the right nodes of the assembly: (a) undeformed configuration; (b) deformed configuration; (c) vertical displacements of the nodes of the auxetic plate initially aligned along horizontal lines indicated in (a).

Fig. 8. Experimental testing facility (a) and image of the auxetic plate in its reference undeformed configuration (b).

Fig. 9. Specimens of auxetic plate with elementary square cells (sketches of the elementary cell and of the assembled plate with details of the gripping system, pictures of the specimens being tested): case of cell length equal to 20 mm, sample A (a), and 15 mm, sample B (b). All dimensions are given in mm.

Fig. 10. Scheme of the interior regions adopted for the definition of a mean value of the Poisson's ratio of the sample: sample A (a), and sample B (b).

Fig. 11. Contour maps of the x- and y-displacements (in mm, a, b) and the corresponding strain fields ε_x, ε_y (c, d) for a mean plate longitudinal strain $\varepsilon_x = 5.6\%$ in sample A.

Fig. 12. Contour maps of the Poisson's ratio for four different levels of the mean plate longitudinal strain ($\varepsilon_x = 2.8\%$ (a), 5.6% (b), 8.5% (c), 14% (d)) in sample A.

Fig. 13. Contour maps of the Poisson's ratio for four different levels of the mean plate longitudinal strain ($\varepsilon_x = 3.3\%$ (a), 5.4% (b), 6.3 (c), 9.7% (d)) for sample B.

Tab. 1. Mean Poisson's ratio for the sample A and B obtained from experiments.

Fig. 14. Beam-like model of the of the auxetic cells by considering rigid node features and detail of the rigid parts of the unit cell (a) (dimensions in mm); comparison of the experimental and FE Poisson's ratio for the sample A (b) and B (c) vs the applied longitudinal deformation with and without considering rigid node features in the FE analyses.

Tab. 2. Average Poisson's ratios for the sample A and B obtained from experiments.

FIGURES AND TABLES

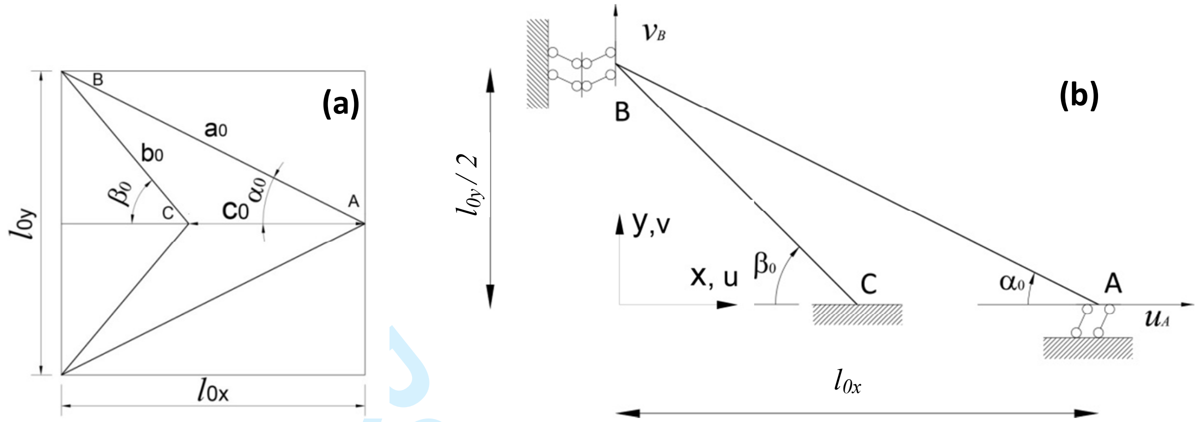

Fig. 1.

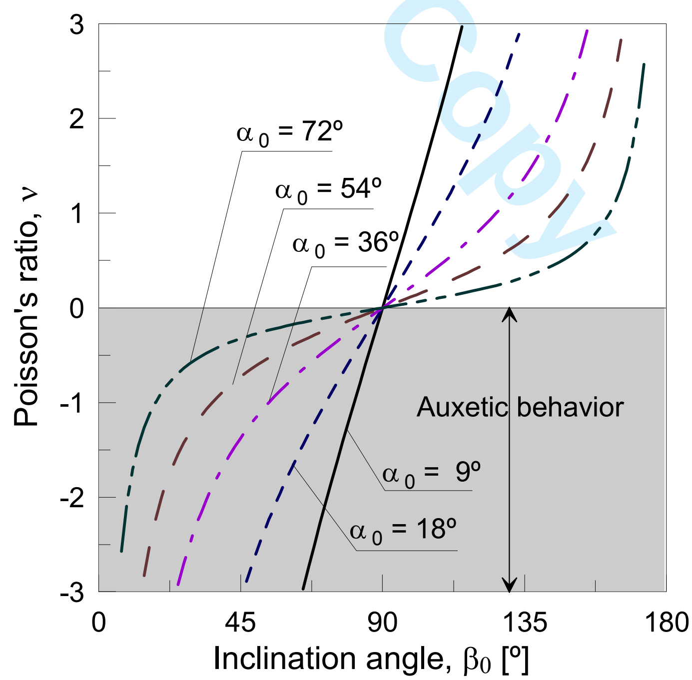

Fig. 2.

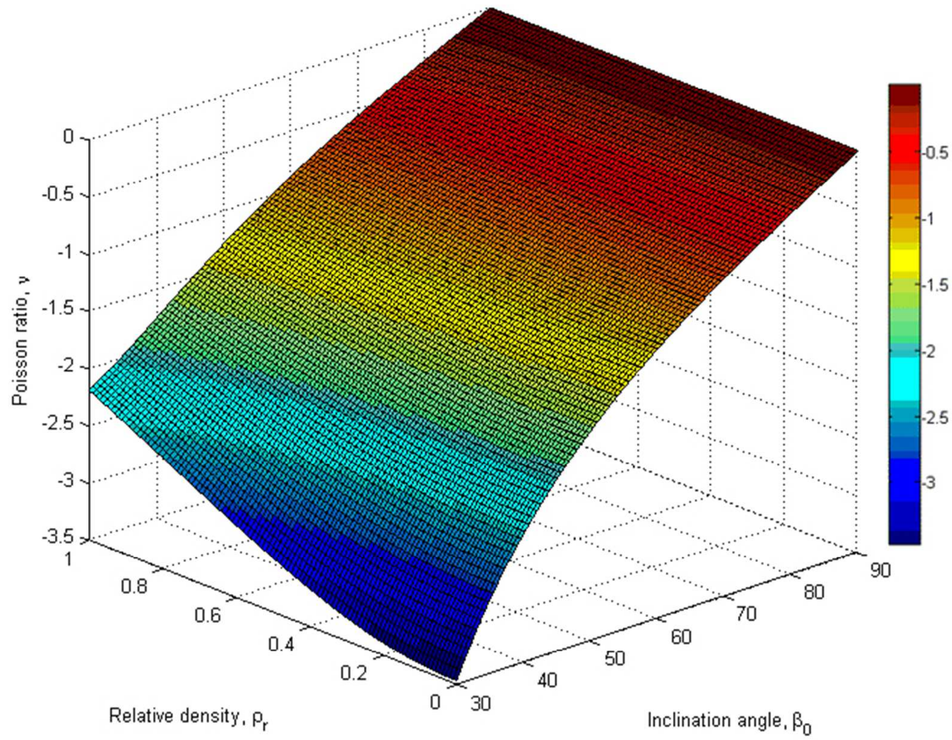
Poisson ratio, ν
Relative density, ρ_r
Inclination angle, β_0
0
-0.5
-1
-1.5
-2
-2.5
-3
-3.5
1
0.8
0.6
0.4
0.2
0
30
40
50
60
70
80
90

Fig. 3.

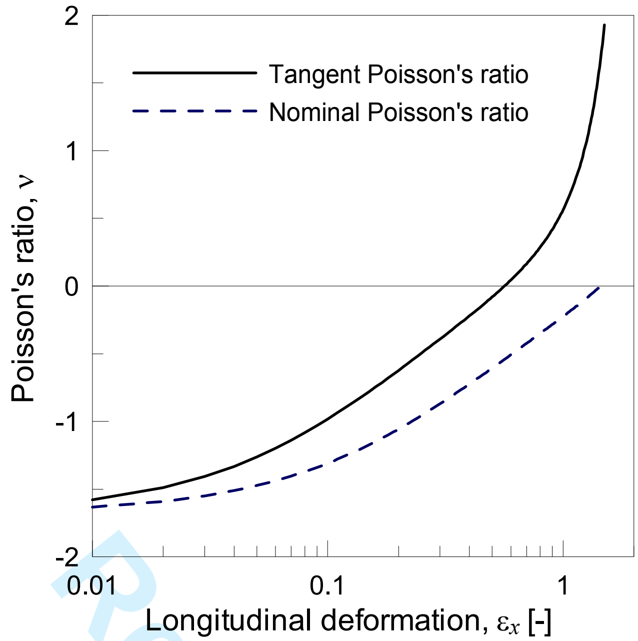

Tangent Poisson's ratio
Nominal Poisson's ratio
Poisson's ratio, ν
Longitudinal deformation, εx [-]
2
1
0
-1
-2
0.01
0.1
1

Fig. 4.

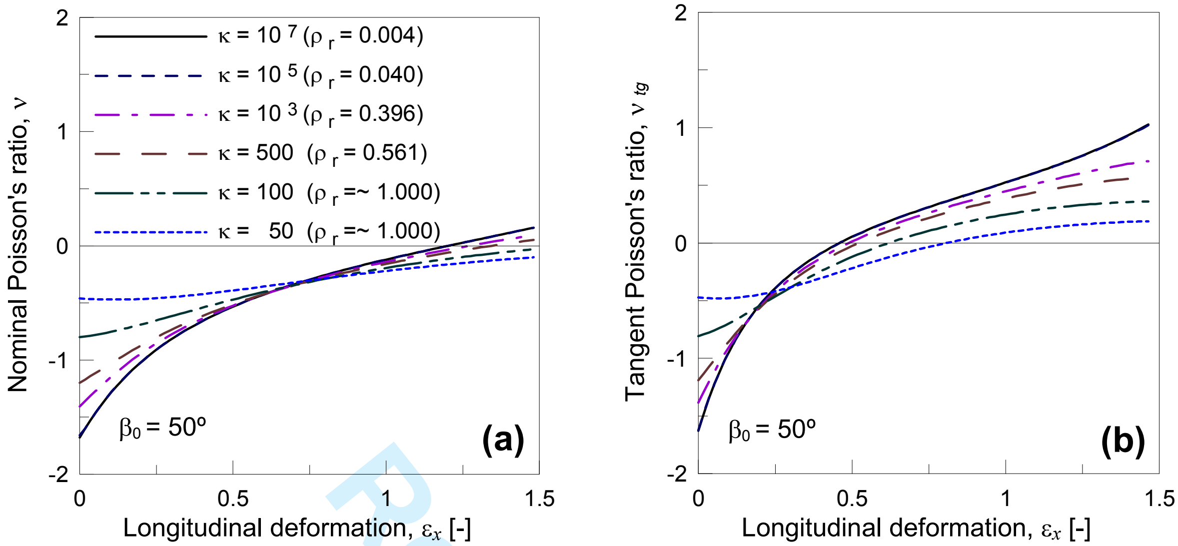
Nominal Poisson's ratio, ν
Tangent Poisson's ratio, ν tg
κ = 10 7 (ρ r = 0.004)
κ = 10 5 (ρ r = 0.040)
κ = 10 3 (ρ r = 0.396)
κ = 500 (ρ r = 0.561)
κ = 100 (ρ r =~ 1.000)
κ = 50 (ρ r =~ 1.000)
β0 = 50º
(a)
(b)
Longitudinal deformation, εx [-]

Fig. 5.

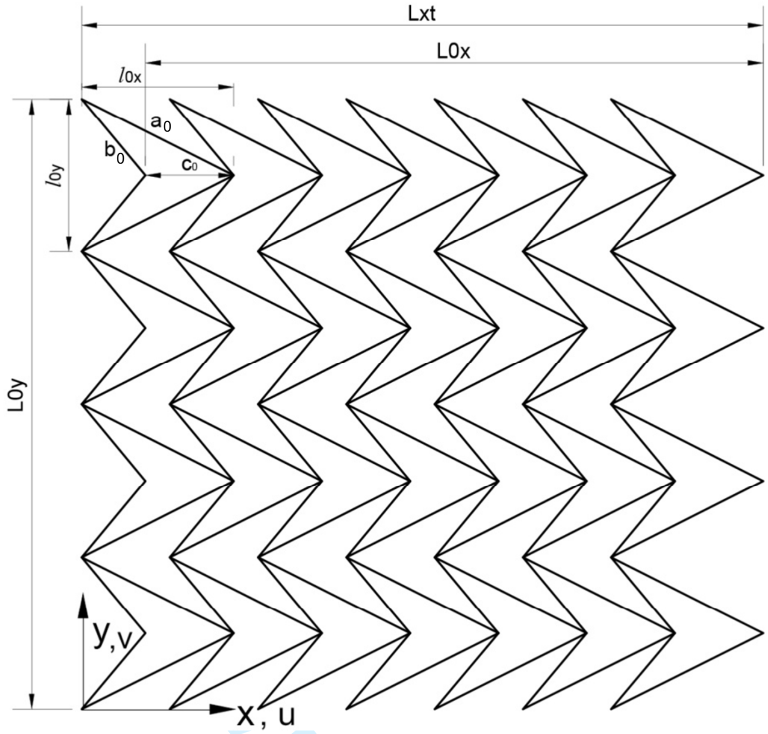

Fig. 6.

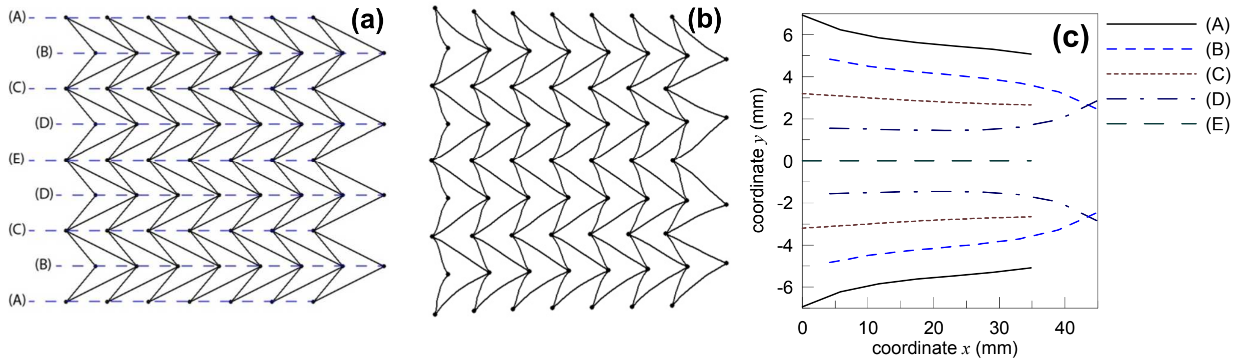

Fig. 7.

(a)

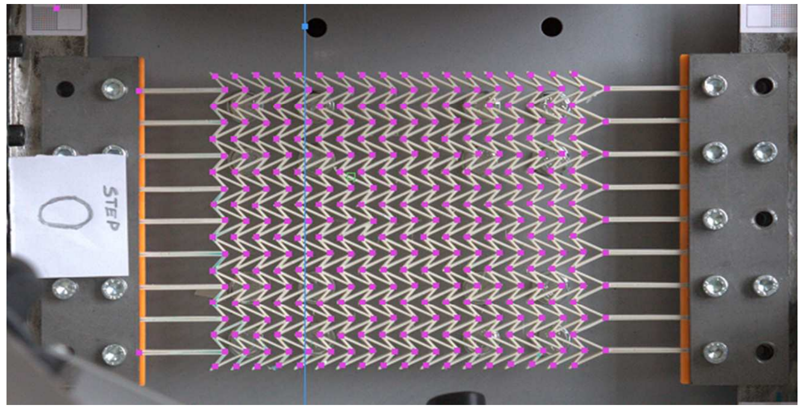

(b)

Fig. 8.

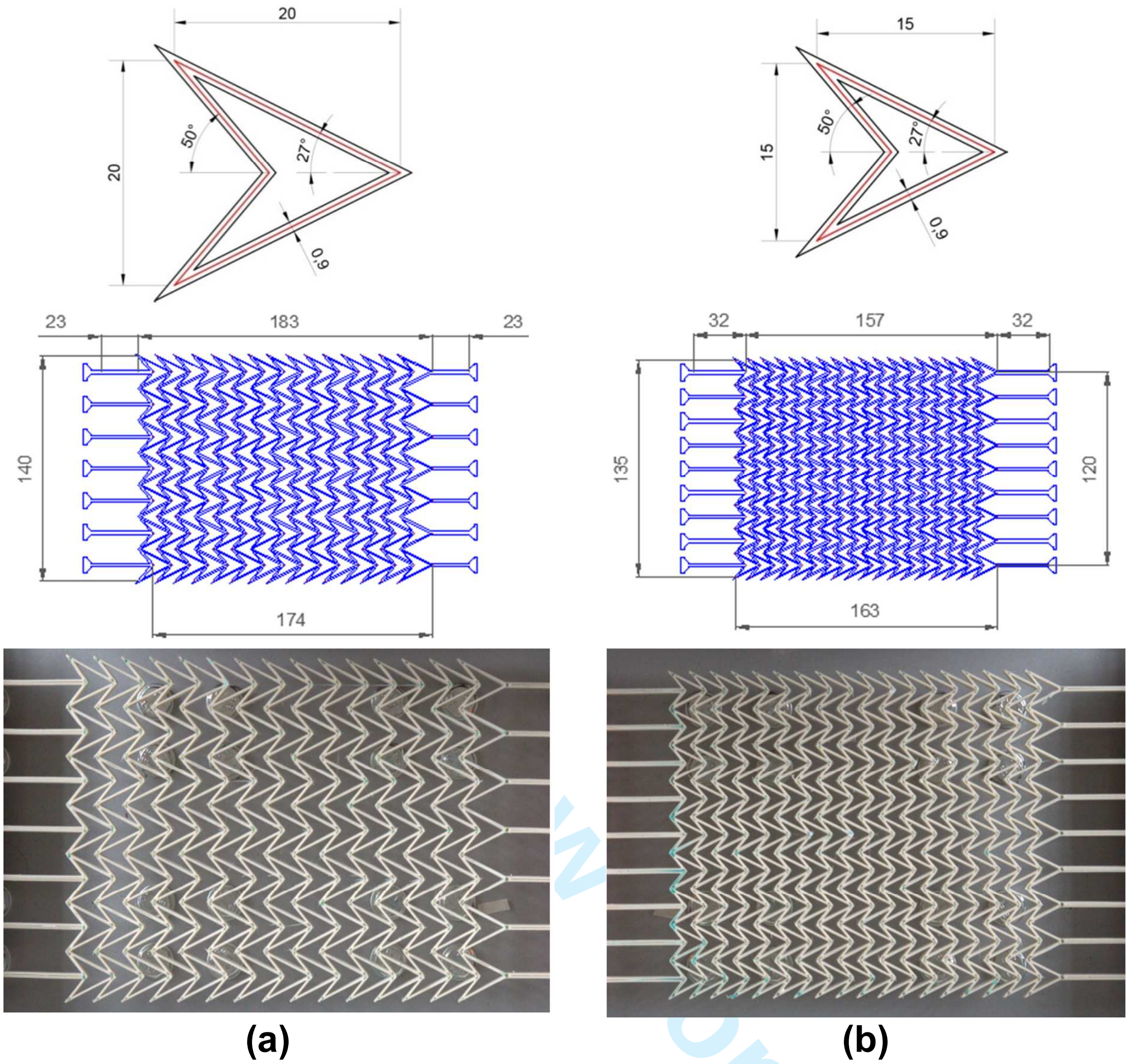
20
20
50°
27°
0.9
15
15
50°
27°
0.9
23
183
23
140
174
32
157
32
135
120
163
(a)
(b)

Fig. 9.

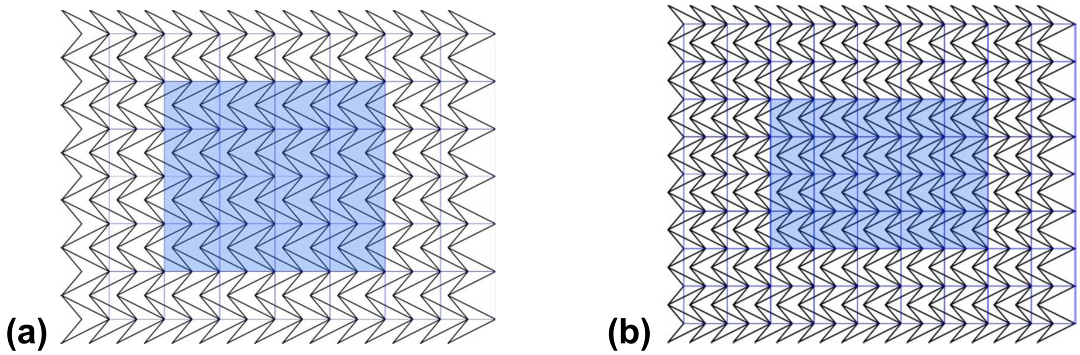

Fig. 10.

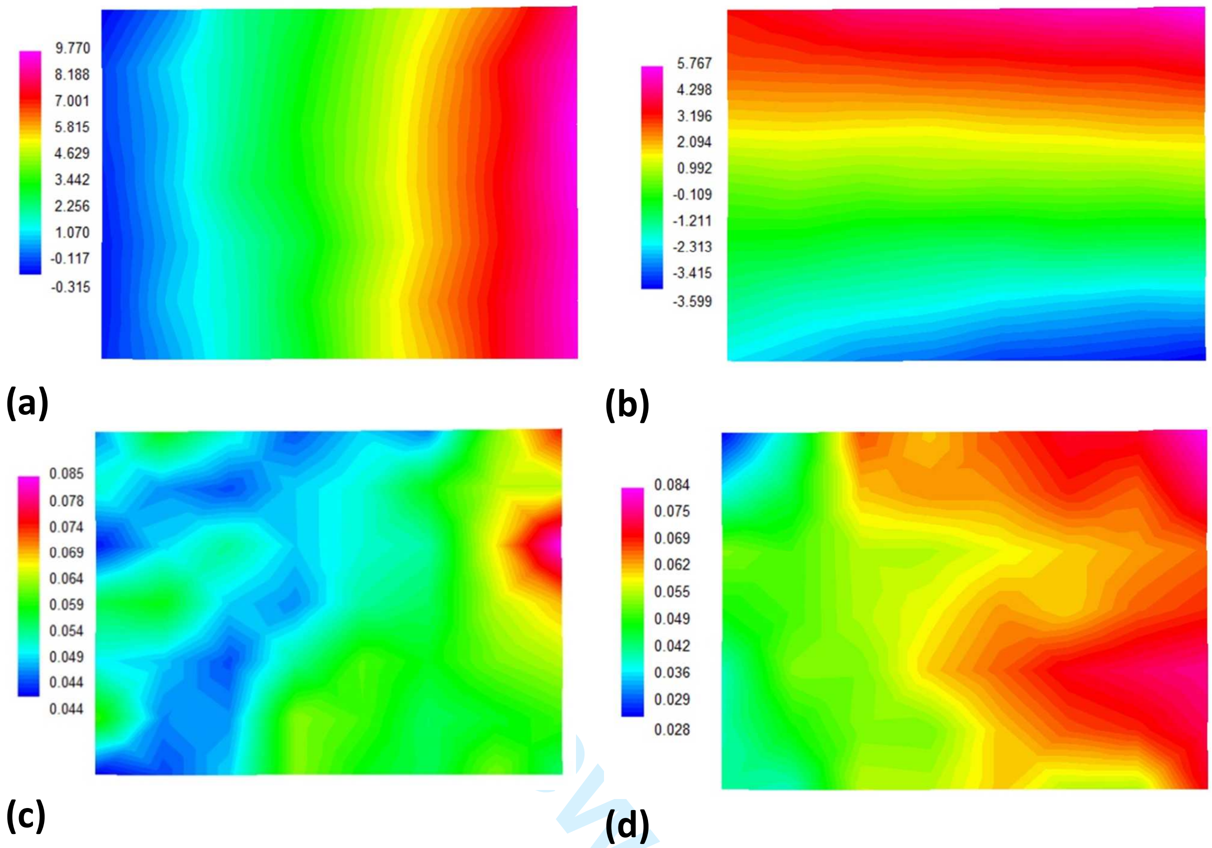
9.770
8.188
7.001
5.815
4.629
3.442
2.256
1.070
-0.117
-0.315
(a)
5.767
4.298
3.196
2.094
0.992
-0.109
-1.211
-2.313
-3.415
-3.599
(b)
0.085
0.078
0.074
0.069
0.064
0.059
0.054
0.049
0.044
0.044
(c)
0.084
0.075
0.069
0.062
0.055
0.049
0.042
0.036
0.029
0.028
(d)

Fig. 11.

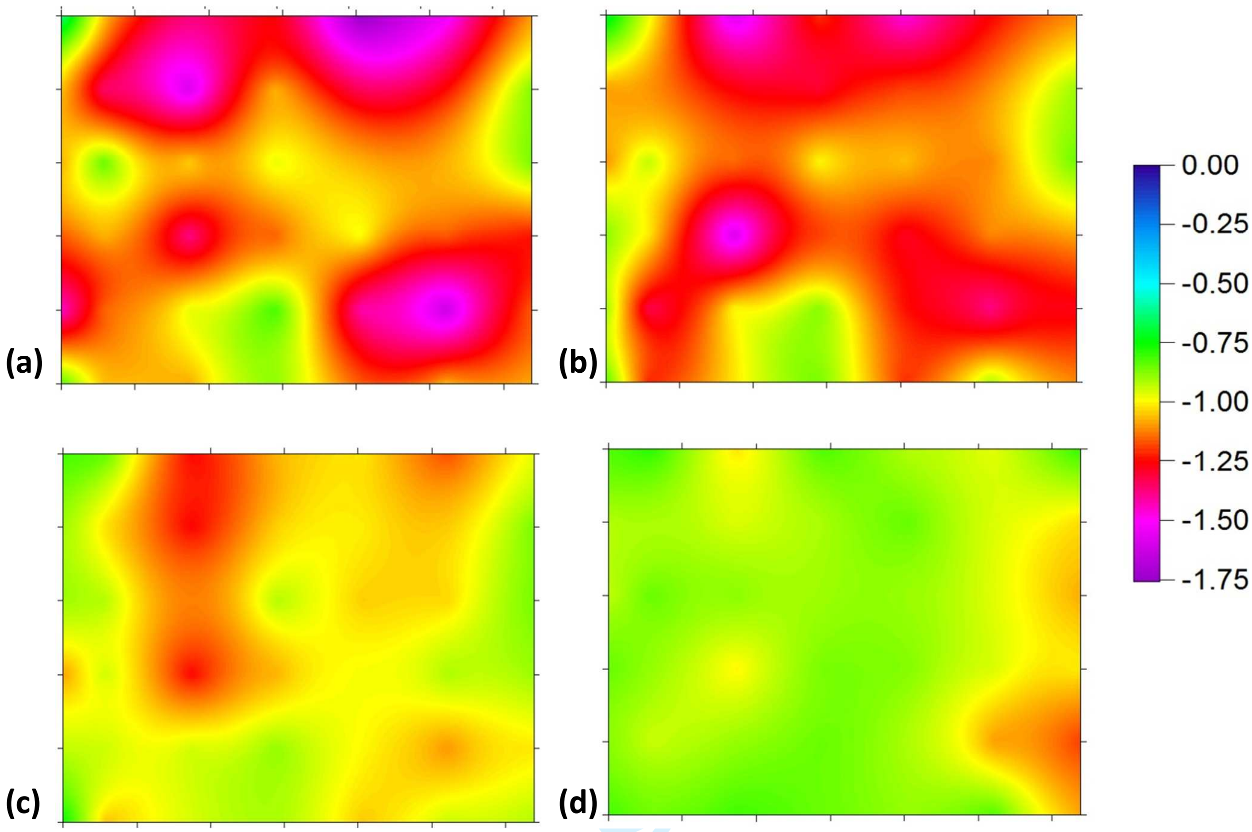

Fig. 12.

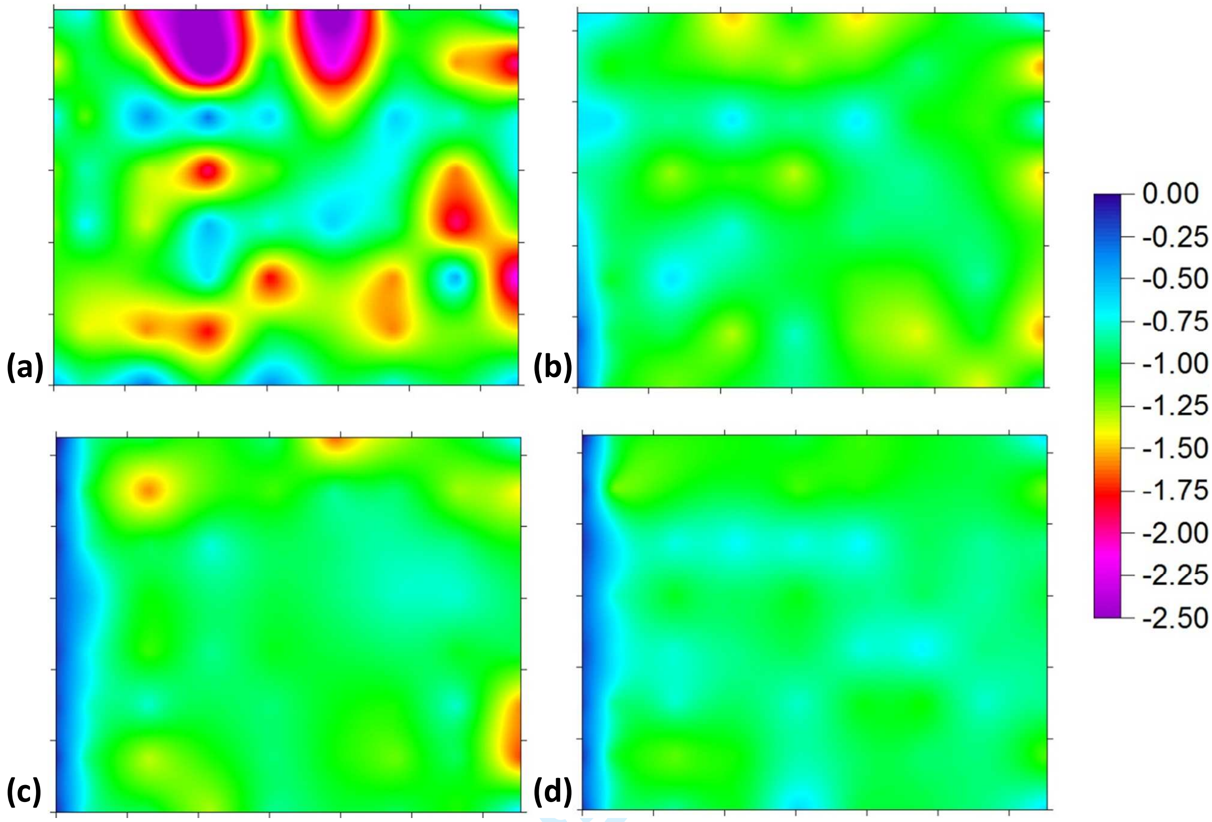

Fig. 13.

Tab. 1.

Sample A		*Sample B*	
ε_x [%]	ν	ε_x [%]	ν
2.8	-1.22	3.3	-0.93
5.6	-1.15	5.4	-0.95
8.5	-1.03	6.3	-0.9
14.0	-0.89	9.7	-0.84

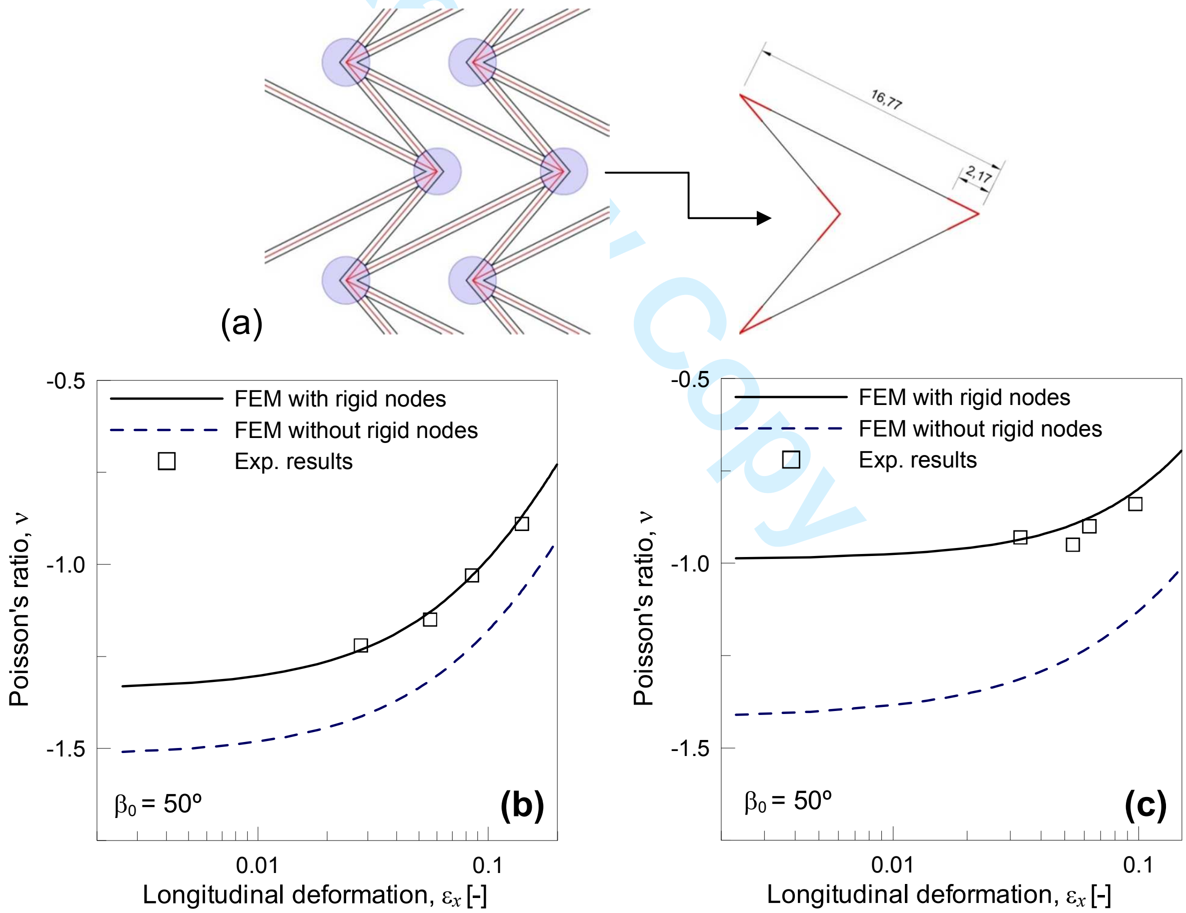

Fig. 14.

Tab. 2.

Sample A					
ε_x [%]	ν	ν (*)	Error %	ν (**)	Error %
2.8	-1.22	-1.41	13.5	-1.23	0.81
5.6	-1.15	-1.15	13.5	-1.15	0.00
8.5	-1.03	-1.23	16.3	-1.04	0.96
14.0	-0.89	-0.96	7.3	-0.87	2.14
Sample B					
3.3	-0.93	-1.32	29.5	-0.94	1.06
5.4	-0.95	-1.26	24.6	-0.9	5.56
6.3	-0.9	-1.23	26.8	-0.88	2.27
9.7	-0.84	-1.14	26.3	-0.81	3.7

** FEM results without rigid nodes; ** FEM results with rigid nodes*